frontiers in Physics

REVIEW
published: 25 May 2020
doi: 10.3389/fphy.2020.00151

In vivo PET/MRI Imaging of the Chorioallantoic Membrane

Gordon Winter[1], *Andrea B. F. Koch*[1], *Jessica Löffler*[1,2], *Fedor Jelezko*[3], *Mika Lindén*[4], *Hao Li*[2,5], *Alireza Abaei*[2], *Zhi Zuo*[2,6], *Ambros J. Beer*[1] *and Volker Rasche*[2,7]*

[1] *Department of Nuclear Medicine, Ulm University Medical Center, Ulm, Germany,* [2] *Core Facility Small Animal MRI, Medical Faculty, Ulm University, Ulm, Germany,* [3] *Institute for Quantum Optics, Ulm University, Ulm, Germany,* [4] *Institute for Inorganic Chemistry II, Ulm University, Ulm, Germany,* [5] *Department of Cardiology, The Second Hospital of Shandong University, Jinan, China,* [6] *Department of Cardiology, Zhongda Hospital, Medical School of Southeast University, Nanjing, China,* [7] *Department of Internal Medicine 2, Ulm University Medical Center, Ulm, Germany*

The Hen's Egg Test Chorioallantoic Membrane (HET-CAM) of fertilized chick eggs represents a unique model for biomedical research. With its steadily increasing use, non-invasive *in ovo* imaging for longitudinal direct quantification of the biodistribution of compounds or monitoring of surrogate markers has been introduced. The full range of imaging methods has been applied to the HET-CAM model. From the current perspective, Magnetic Resonance Imaging (MRI) and Positron Emission Tomography (PET) appear promising techniques, providing detailed anatomical and functional information (MRI) and excellent sensitivity (PET). Especially by combining both techniques, the required sensitivity and anatomical localization of the signal source renders feasible. In the following, a review of recent applications of MRI and PET for *in ovo* imaging with a special focus on techniques for imaging *xenotransplanted* tumors on the CAM will be provided.

Keywords: HET-CAM, MRI, PET, imaging, biodistribution, targeting

OPEN ACCESS

Edited by:
Claudia Kuntner, Austrian Institute of Technology (AIT), Austria

Reviewed by:
Violaine See, University of Liverpool, United Kingdom
Anne Herrmann, University of Liverpool, United Kingdom

***Correspondence:**
Volker Rasche
volker.rasche@uni-ulm.de

Specialty section:
This article was submitted to Medical Physics and Imaging, a section of the journal Frontiers in Physics

Received: *02 December 2019*
Accepted: *15 April 2020*
Published: *25 May 2020*

Citation:
Winter G, Koch ABF, Löffler J, Jelezko F, Lindén M, Li H, Abaei A, Zuo Z, Beer AJ and Rasche V (2020) In vivo PET/MRI Imaging of the Chorioallantoic Membrane. Front. Phys. 8:151. doi: 10.3389/fphy.2020.00151

INTRODUCTION

The Hen's Egg Test Chorioallantoic-Membrane (HET-CAM) of fertilized chicken eggs represents a unique model for biomedical research. During the development, the mesodermal layers of the allantois and chorion form the chorioallantoic membrane (CAM). This structure forms a rich vascular network enabling to study tissue grafts, tumor growth, metastasis formation, wound healing, drug delivery, toxicologic analysis, angiogenic and anti-angiogenic molecules [1].

The HET-CAM represents a relatively simple, quick, and low-cost model that allows screening of a large number of pharmacological samples in a short time. It has been successfully used to study cancer progression and its pharmacological treatment [2–8], angiogenesis [9], pharmacokinetics [10], properties of novel nanomaterials [9, 11], or as a model system to study microsurgical instruments and techniques [12]. Especially for xenotransplantation tumor models, the HET-CAM offers various advantages in comparison to the murine models. Since the development of the lymphoid system starts in the late stage of incubation, the HET-CAM model represents a naturally immunodeficient host, enabling xenotransplantation of many kinds of tumors without species-specific limitations [11]. The blood vessel network of the CAM thereby provides an excellent environment for primary tumor formation and a basis for angiogenic blood vessel formation [12]. Human cell line derived [13] xenografts are considered an increasingly valuable tool in oncology potentially providing biologically models of many different cancer types. Where immunodeficient rodent models

pose barriers to widespread application due to cost and efficiency constraints, the HET-CAM model renders as efficient model especially for initial testing of tumor progression [10, 14–16], in many countries not requiring any approval for animal experiments, if sacrificed before hatching.

Due to its simplicity, the HET-CAM model appears as ideal platform for initial testing of pharmacological compounds and tissue properties, including biodistribution assessment or efficacy assessment of new compounds [1, 8, 13–19].

With the increasing use of the HET-CAM model and the need for longitudinal monitoring, non-invasive *in ovo* imaging of the chick embryo and especially the CAM has gained interest over recent years. Optical methods like optical coherence tomography (OCT) and Doppler techniques have successfully been applied for deriving functional and physiological properties of the embryo [20–38]. Three-dimensional microcomputed tomography (μCT) has been applied *in ovo*, especially in the field of bone volume and mineral density assessment [39–46]. With the recent advances in magnetic resonance tomography (MRI) its application to *in ovo* imaging has rendered feasible and many applications of the technique in the live embryo as well as after sacrification have been reported for different scientific fields, including embryonal development [47–54], ophthalmology [48–57], oncology [58–63], metabolic assessment [54, 64], and initial testing of the biodistribution of new compounds [65–67]. Further, nuclear imaging methods have been translated to *in ovo* imaging, mainly for initial testing of new labeling strategies [19, 68–71].

Considering the capability of the HET-CAM model for monitoring the growth and progression of xenotransplanted tumors rises a huge potential for its use in the evaluation of the biodistribution of new compounds, especially in combination with specific targeting strategies. In this context the combination of the multi-contrast capabilities of MRI with the outstanding sensitivity of positron emission tomography (PET) appears promising. In the following a review of recent applications of MRI and PET for *in ovo* imaging with a special focus on techniques for imaging xenotransplanted tumors on the CAM will be provided.

THE HET-CAM MODEL

In preclinical research and drug development can-cer cell lines (CCL) are frequently used. However, in culture, CCLs often fail to retain morphology, cellular heterogeneity, and molecular profiles of the donor tissue [72, 73], and drug performance in xenografts may not perfectly reflect clinical efficacy [74]. The success of new drugs in oncology requires preclinical models that render the full heterogeneity and pathophysiology of patient tumors, and CCL or patient-derived xenografts (PDX) may mimic physiological drug effects [75, 76].

A broad range of applications for CCL and PDX have been reported using rodent models as host and their efficient use in prediction of response, development of biomarkers, and monitoring and identification of efficient treatment regimens has been proven [77]. Despite their frequent use, rodent models have practical and scientific limitations. In many applications, rodent models have shown a very limited success rate in engraftment. Successful engraftment often takes several months. Further high, often prohibitive costs and resources are required for keeping rodents in an appropriate facility under proper hygienic conditions. They are labor-intensive, time-consuming, and require ethical approval by the regulatory authorities.

The HET-CAM model represents a well-established alternative *in vivo* assay. It presents a highly vascularized extra-embryonic membrane, which is connected to the embryo through a continuous circulatory system. Even though T and B cells can be detected in the chick embryo immune system by embryo development day (EDD) 11 and 12, full immune competence is not developed until EDD 18 [16]. The HET-CAM is a low-cost model with the limita-tion of developing a nonspecific inflammatory response after EDD 15 [1]. Xenotransplantation and growth of cancer cell lines on the CAM is well-established (**Figure 1**) and has amongst others been applied for initial assessment of the efficacy of anticancer drugs [78]. Compared to the rodent models, tumor formation on the CAM is fast, with graft vascularization and thus interface to the chick embryo vascular system normally established already after 2-5 days [79].

For xenotransplantation, fertilized chicken eggs e.g., White Leghorn (*Gallus domesticus*) are purchased from a hatchery and maintained at 37.8°C and a 60% relative humidity atmosphere for the whole incubation period. Upon arrival the eggs are carefully cleaned (e.g., by 70% ethanol solution) and incubation is started (EDD 0). After 4 days (EDD 4) of incubation the eggs are fenestrated and analyzed for fertilization by visual assessment of the CAM vascularization and heartbeat of the embryo. The shell access window is sealed to prevent contamination and the egg placed back into the incubator. Cancer cells are seeded on the CAM and a solid tumor, well interfaced to the extra-embryonic vascular system, forms within few days [1, 16]. The viability of the embryos needs to be monitored daily by checking the CAM vasculature for blood flow, physiological embryo movement, and the growth of the chick embryo according to Hamburger and Hamilton [80].

MAGNETIC RESONANCE IMAGING (MRI)

With its versatile image contrast, MRI raised interest in imaging of chick embryos already in the 80s. In 1986, Bone et al. [81, 82] reported first three-dimensional MR microscopy on the live chick embryo. At a 1.5T prototype system with dedicated gradient system and receive coil, they achieved a spatial resolution of 200 x 200 x 1200 μm^3 with T1 and T2 weighting, applying partial saturation (PS) and spin echo (SE) 3D-Fourier imaging techniques (3D-FT). To minimize motion-induced image artifacts, the chick embryo was immobilized by placing the egg in ice chips between 20 (EDD 11) and 90 (EDD 15) minutes. Imaging was performed at room temperature. Even though the spatial resolution and hence the fidelity of the anatomical details was still limited, Bone et al. clearly showed the potential combination of *in ovo* imaging and MRI as basis for further MRI studies. Improvements in spatial resolution were

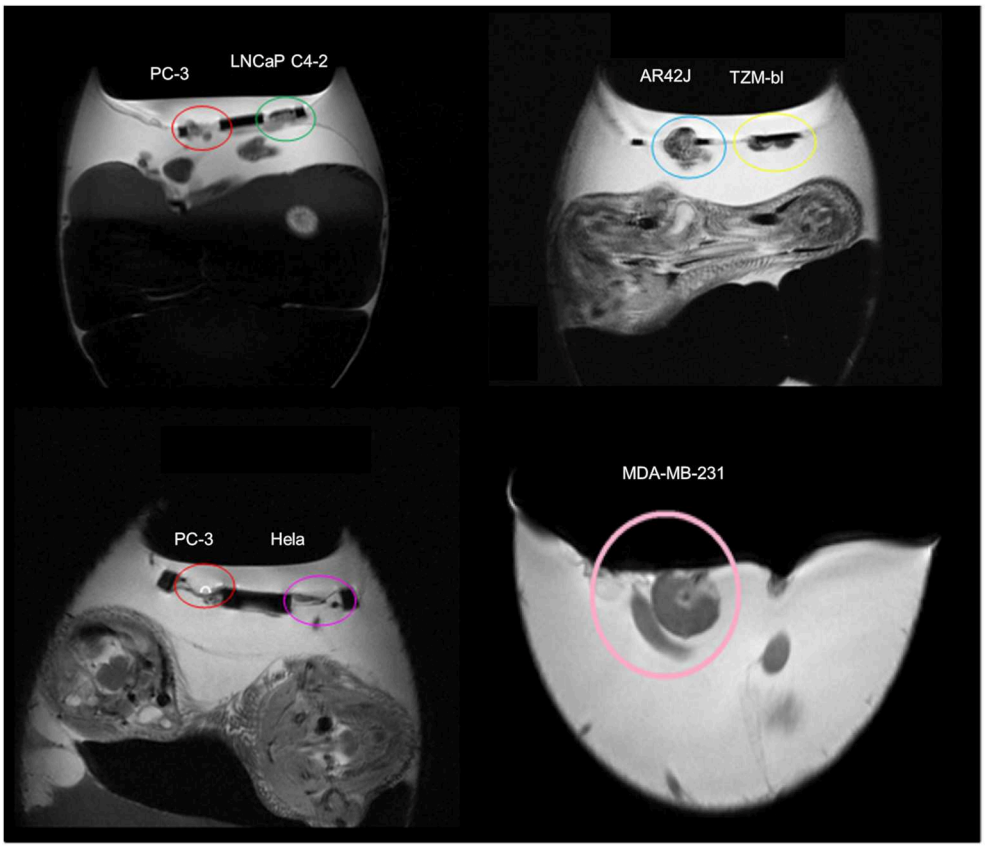

FIGURE 1 | Magnetic resonance images (MRI) of xenotransplanted tumors grown on the chorioallantoic membrane (CAM) from different cell lines (prostate cancer: PC-3, LNCaP C4-2; pancreas cancer: AR42J; adenocarcinoma: TZM-bl; cervical cancer: HELA; breast cancer: MDA-MB-231). Unpublished imaging material provided by Winter and Li.

reported by Effmann et al. [83], who used an implantable 18 mm diameter RF coil wrapped around the chick embryo, inductively coupled to an outside MR receiver [84]. With the resulting gain in signal-to-noise ratio (SNR), the PS 3D-FT could provide images with spatial resolutions of up to 50 x 50 x 600 μm^3 within 1-2 h scan times.

Assessment of metabolic developments by phosphorus ^{31}P MR spectroscopy (MRS) in correlation with anatomic developments were first reported by Moseley et al. in 1989 [54], who could clearly demonstrate the decrease of the observable ^{31}P volume by 80% indicating the respective tissue uptake. Further spectroscopy work was performed by Lirette et al. [85] for longitudinal quantification of the fat/water ratio (^{1}H MRS) and the phosphormono-/phosphordiester ratio (^{31}P MRS). Data were acquired with a 5 cm—diameter surface coil, in which the eggs were placed centrally. Acquisition times were below 1 h. Embryo motion was controlled by applying 1–2% halothane during scanning. Peebles et al. [86] applied ^{1}H MRS for monitoring of brain metabolites and diffusion MRI for assessment of changes in the apparent diffusion coefficient (ADC) in the brain during hypoxia. Immobilization of the chick embryo was achieved by dropping 5.0 mg Ketamine onto the CAM. Single voxel MRS of 6 x 6 x 6 mm^3 volumes of interest were acquired in about 30 minutes acquisition time, with subsequent acquisition of the diffusion MRI by a two-point method with 230 x 230 x 2000 μm^3 resolution.

Falen et al. [53] and Hutchison et al. [87] applied MRI with T1 and T2—weighted imaging techniques to the assessment of the yolk structure. Both reported the applicability of MRI for the assessment of the morphology of yolk, albumen, air space, and eggshell. The inner structure of the yolk, including concentric yolk rings, could be clearly visualized by this non-destructive imaging technique. In 2000, Donoghue et al. [88] reported the application of MRI for monitoring residue transfer into egg yolk. After injection of Gd-DTPA, the transfer of the drug into the yolk was monitored by scanning the egg applying a T1-weighted (MP-RAGE) sequence. It could be shown that Gd-DTPA residues were incorporated into the yolk ring structure.

Assessment of the chick embryo vasculature by MRI was reported by Smith et al. in 1992 [89]. They performed *ex vivo* high-resolution MRI of the embryonic vasculature after perfusion fixation of the vasculature structure with gadolinium-doped gelatin. A similar approach was chosen by Hogers et al. [52] to demonstrate the benefit of ultra-highfield imaging by

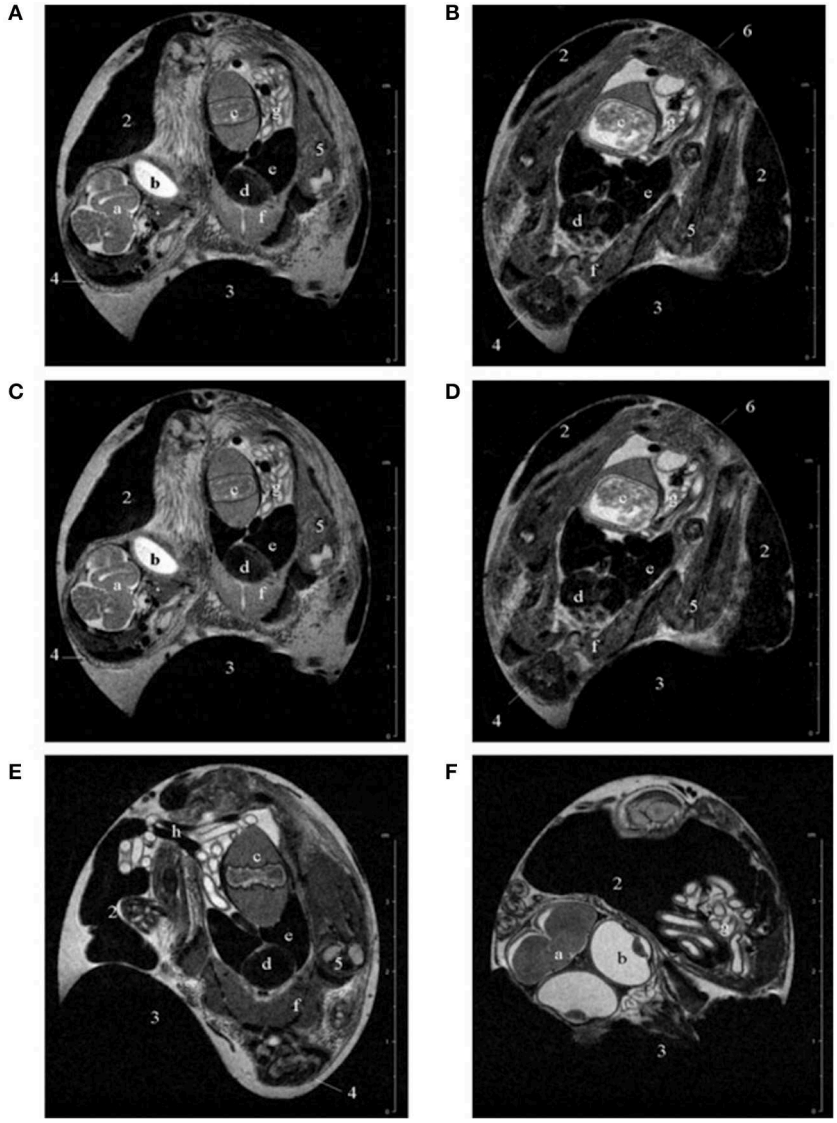

FIGURE 2 | Representative examples of T2-weighted multislice scans of chick embryos in ovo at **(A)** 12, **(B)** 15, **(C)** 17, **(D)** 18, **(E)** 19, and **(F)** 20 days of incubation. 1, albumen; 2, yolk; 3, air sac; 4, head; 5, limb; 6, rump; a, brain; b, eye; c, gizzard; d, heart; e, liver; f, pectoral muscles; g, intestine; h, umbilical vessels. The complete scans can be viewed at www.gla.ac.uk/7tmr/chickegg.htm. This research was originally published in JMRI: Noninvasive Monitoring of Chick Development In Ovo Using a 7T MRI System From Day 12 of Incubation Through to Hatching. Bain et al. [51].

comparing MRI *in vitro* microscopy between 7T and 17.6T field strength. A similar *ex vivo* technique was applied by Zhang et al. [90] and Yelbuz et al. [91, 92], who used the combination of perfusion with immersion fixation and a small molecular gadolinium agent to improve image contrast between the myocardial wall and heart lumen. Isotropic three-dimensional images with up to 25^3 μm^3 spatial resolution were acquired with a T1-weighted spin warp technique in about 29 h scan time at 9.4T field strength. *In ovo* quantification of the cardiac function was reported by Holmes et al. [93, 94] applying a self-gating technique for cardiac synchronization of the data. Even though adequate image quality could be obtained, the authors identified the bulk embryo motion at earlier stages as main limiting factor for reproducible image quality.

Noninvasive monitoring of chick embryo development was reported by Bain et al. [51] in 2007. For optimal image contrast a T2-weighted spin echo technique (RARE) was applied yielding 195 x 195 x 500 μm^3 spatial resolution within 25 minutes scan time at 7T (**Figure 2**). Rapid three-dimensional T1-weighted techniques provided higher spatial resolution, but organ contrast was not sufficient. For chick embryo immobilization, Bain et al. [51] used a precooling protocol, keeping the chicken eggs at

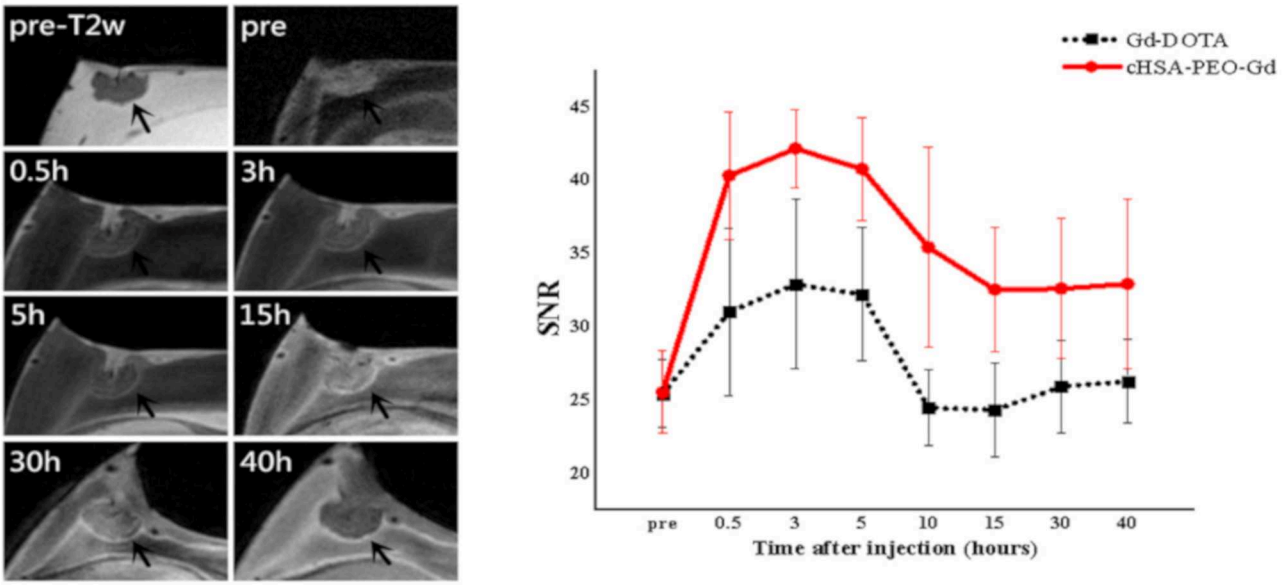

FIGURE 3 | Representative MR images of cHSA-PEO(2000)16-Gd biodistribution in solid tumor (left) and comparison of the SNR (Signal-to-Noise Ratio) of the tumor (right) over the first 40 h after systemic injection of cHSA-PEO(2000)16-Gd and Gd-DOTA. This research was originally published under the terms of the CC BY license (Creative Commons Attribution 4.0 International License) in Sci Rep: The CAM cancer xenograft as a model for initial evaluation of MR labeled compounds. Zuo et al. [65].

4°C for 60 min prior to data acquisition with subsequent data acquisition at room temperature. No slowdown or arrest of the chick embryo development was observed by the cooling or the MRI examinations. As alternative cooling protocol, Li et al. [95] suggested data acquisition at 19°C thus enabling scan times of up to 4 hours in quail embryos. More advanced imaging techniques including T1 and T2 mapping as well as magnetization transfer ratio (MTR) quantification were reported by Boss et al. [50]. Motion reduction was achieved by application of 0.5 mL Ketamine onto the CAM. Images were acquired with two-dimensional multi-slice techniques at a spatial resolution of 180 x 180 x 1000 μm^3 (T1), 260 x 260 x 1000 μm^3 (T2), and 230 x 230 x 1000 μm^3 (MTR). In 2015, Zhou et al. [49] translated developmental imaging of the brain to a 3T clinical scanner equipped with a dedicated small animal coil. T2 weighted RARE images as well as DTI data could be acquired at reasonable spatial resolution (T2w: 170 x 170 x 1000 μm^3 in 8 minutes, DTI: 1.25 x 1.25 x 1 mm^3 in 6 minutes), enabling noninvasive analysis of brain development including structural information. Imaging of the chick embryo brain development after Zika virus infection was reported by Goodfellow et al. [96], who could clearly demonstrate Zika virus induced microcephaly. High-resolution MRI at 7T were presented by Lindner et al. [48] for monitoring the chick embryo eye development. Immobilization of the embryo was achieved by bedding the egg on crushed ice ten minutes before scanning.

A first application of *in ovo* MRI for the assessment of the biodistribution of new compounds was reported by Dingman et al. [97] in 2003. They longitudinally investigated the distribution of a 19F-labeled L-6-heptafluorobutyryl-5-hydroxytryptophan including uptake dynamics and crossing of the blood-brain barrier. In 2007, Oppitz et al. [98] suggested the use of chick embryo model for evaluation of the advantages and limitations of MRI to monitor the migration of superparamagnetic iron oxide (SPIO) labeled cells. A similar approach was presented by Pereira et al. [99] who showed in the chick embryo model an improved sensitivity for *in vivo* cell tracking after implantation by supplementing the culture medium with adequate iron sources as compared to the use of reporter genes. Faucher et al. [100] used the HET-CAM model for initial investigation of ultra-small gadolinium oxide nanoparticles for labeling of glioblastoma cells, seeded on the CAM. Taylor et al. [101] used the chick embryo model for initial evaluation of new nano- and micro-sized magnetic particles for cell tracking. All imaging was performed *ex vivo*. In 2017, Zuo et al. [65] reported the use of human cancer cell lines xenotransplanted onto the CAM for initial assessment of the biodistribution of MR labeled drugs. After injection of Gd-DOTA, the biodistribution of the compound in the chick embryo as well as in the xenotransplanted tumor was observed. By longitudinal imaging studies over 40 h, the accumulation and clearance of the contrast agent could be monitored. The technique was applied for demonstrating the feasibility of the HET-CAM tumor model for monitoring the fate of new MR labeled drugs by following the image contrast after intravenous administration of a gadolinium-labelled polymeric nanoparticle at high spatial resolution, applying an immobilization protocol as suggested earlier [61]. In direct comparison with conventional contrast agents, a significantly prolonged retention time of the polymeric nanoparticle in the tumor could be shown (**Figure 3**). For assessment of the intra-tumor distribution, 3D T1 weighted data were acquired at high spatial resolution of 100 x 100

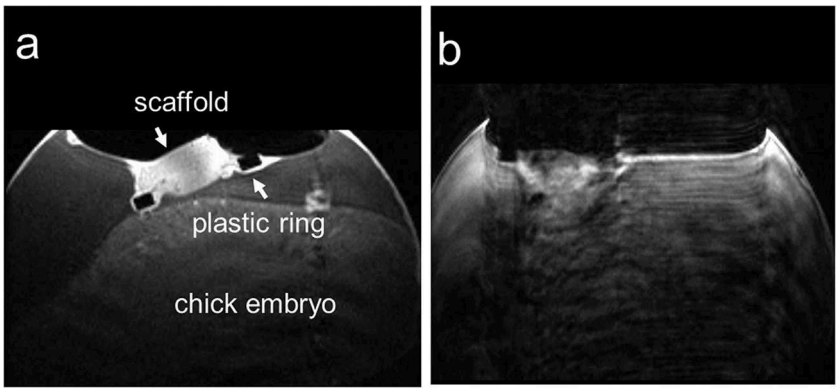

FIGURE 4 | Two in ovo T1-weighted MR images of the chick embryo on ID 14, seven days post-implantation on the CAM acquired in an axial slice through the biomaterial scaffold; **(a)** image without motion artifact and **(b)** image with motion artifacts that was excluded from further analysis. This research was originally published under the terms of the CC BY license (Creative Commons Attribution 4.0 International License) in Sci Rep: Comparison of medetomidine, thiopental and ketamine/midazolam anesthesia in chick embryos for in ovo Magnetic Resonance Imaging free of motion artifacts. Waschkies et al. [106].

x 560 μm^3. Hafner et al. [102] used a similar approach for initial evaluation of the biodistribution of a multifunctional drug carrier.

Buschmann et al. [103] reported implantation of human osteoblasts-seeded scaffolds onto the CAM. One week after xenotransplantation, MRI (T1, T2 quantification) analysis was performed *ex vivo*, after intravenous injection or dripping of gadolinium onto the scaffold before sacrificing the embryo allowing for the analysis of the formation of new capillaries. The published *ex vivo* data clearly indicated the potential of the HET-CAM model as cheap reliable model for monitoring the angiogenesis in tissue-engineering. This work was further developed by Chesnick et al. [104] by initial testing of a new adrenolate labeled gadolinium complex for specific targeting to bone mineral. In 2015, Pfiffner et al. [105] presented *in vivo* MRI at 4.7T to noninvasively quantify and monitor the perfusion capacity in the HET-CAM model. After placing a biomaterial on the CAM, its perfusion capacity was quantified by relaxation rate changes after intravenous injection of the gadolinium-based contrast agent. Immobilization of the chick embryo was achieved by 5 drops of ketamine 1:100 (Ketasol-100, Graeub, Switzerland) dripped onto the CAM surface. Anatomical reference images were obtained applying a FLASH sequence at measured spatial resolution of roughly 500^2 μm^2. T1 and T2 maps were derived applying RARE sequences with multiple repetition times (TR) and echo times (TE) at spatial resolution of 200 x 200 x 1000 μm^3 before and at different time points after intravenous injection of 100 μL Gd-DOTA (0.5M) MRI contrast agent. Relaxation rate changes over the scaffold could be clearly assessed indicating different vascular density, which was confirmed by histology.

Motion artifacts introduced by bulk motion of the chick embryo is a major limiting factor for high-resolution imaging of the CAM (**Figure 4**). In 2015, Waschkies et al. [106] investigated the use of different anesthesia drugs for immobilization, whereas Zuo et al. [61] evaluated an age-adjusted precooling protocol for high-resolution imaging of the CAM. In Waschkies *et al*, medetomidine at a dosage of 0.3 mg/kg, was compared to thiopental at 100 mg/kg and ketamine/midazolam at 50 and 1 mg/kg. The soluble anesthetics were applied by dropping a total volume of 0.3 mL onto the surface of the CAM. It was demonstrated that medetomidine performed best, enabling motion-free MRI for a period of about 30 min starting 10 min after application. Ketamine/midazolam yielded insufficient depth of anesthesia and thiopental anesthesia did not immobilize the chick embryo sufficiently long. In contrast, Zuo et al. investigated the use of an anesthesia-free immobilization approach. As extension to earlier published work [51], they suggested adaptation of the precooling time according to the age of the chick embryo, thereby achieving almost complete immobilization of the chick embryo for at least 60 min thus allowing multi-contrast high-resolution imaging of the chick embryo and xenotransplanted tumors on the CAM (**Figures 5**, **6**). The suggested cooling protocol allowed *in vivo* imaging at high spatial resolution as 77 x 91 x 500 μm^3 (T2 weighted anatomic, 2D), 200 x 200 x 500 μm^3 (diffusion weighted, 2D), 104 x 98 x 500 μm^3 (T2 mapping, 2D), and 100 x 100 x 560 μm^3 (T1 weighted, 3D). Tumor volume and growth could be monitored longitudinally from day 4 to day 9 after xenotransplantation. The tumor progression could be monitored for each individual case (**Figure 7**) and the volumes derived from MRI at day 9 excellently correlated with the respective volumes derived after resection of the tumors. In 2018, Herrmann et al. [58] reported the application of MRI to measure primary neuroblastoma tumor size and metastasis in a chick embryo model. Human neuroblastoma cells labeled with green fluorescent protein (GFP) and micron-sized iron particles were xenotransplanted on the CAM at EDD 7. At EDD 14, T2 RARE and T2-weighted fast low angle shot (FLASH) data were acquired (**Figure 8**) using the cooling protocol as suggested by Zuo et al. [61]. Additionally, Herrmann et al. performed time-of-flight (ToF) MR angiography (MRA) and reported a reduced blood flow if using the cooling protocol, making successful ToF acquisition unfeasible. Instead, ketamine anesthesia (3.6 mM ketamine in 500 μL PBS) was applied resulting in MRI data free

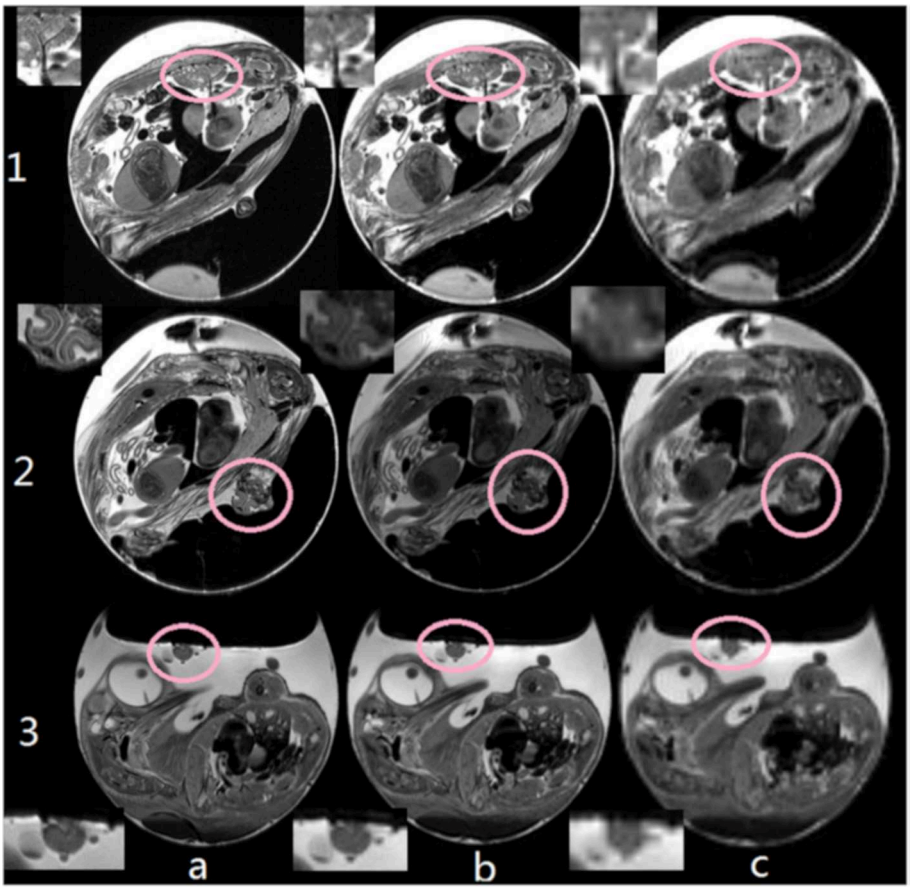

FIGURE 5 | Comparison between different image resolution: **(a)** 77 × 91 μm^2, **(b)** 200 × 200 μm^2, and **(c)** 500 × 500. With increasing resolution, details of e.g., the pulmonary veins (1), the beak (2, axial orientation), and tumor tissues (3) could be clearly resolved. Insets show details of the respective target structures. This research was originally published in NMR Biomed: High-resolution MRI analysis of breast cancer xenograft on the chick chorioallantoic membrane. Zuo et al. [61].

of motion artifacts for a period of 30 min. The micron-sized iron labeling of the cells allowed *in ovo* assessment of the primary tumor and detection of metastatic deposits.

POSITRON EMISSION TOMOGRAPHY (PET)

Most anatomic and functional imaging of the HET-CAM model has been performed by MRI so far. The main limitation of PET results from its rather low spatial resolution, which does not fit the high spatial resolution demands for imaging of the CAM. To gain from the outstanding sensitivity of PET, thus in almost all work published, PET (or SPECT) imaging was complimented by Computer Tomography (CT), x-ray, or MRI for providing additional anatomic details.

In 2012, Würbach et al. [71] introduced using ^{18}F-fluoride PET for assessment of bone metabolism. For radionuclide injection, a self-built catheter made of a 30G needle and a polythene tube with 0.28 mm inner diameter was introduced into one of the CAM vessels. Imaging was performed for a period of roughly 75 minutes yielding dynamic images (55 time frames) as well as high-quality static data. Applying an iterative ordinary Poisson maximum *a posteriori* reconstruction yield voxel sizes of roughly 400 x 400 x 800 μm^3. The results proved the quantitative and reproducible assessment of bone metabolism in anesthetized chick embryos. Immobilization of the chick embryo during scanning was achieved by exposing the CAM to isoflurane at 1.5% concentration as suggested by Heidrich et al. [107], who investigated different anesthesia schemes for *in vivo* imaging of avian embryos, including isoflurane, 2,2,2-tribromoethanol (Avertin), and urethane/α-chloralose (UC). UC and Avertin were directly applied as liquids onto the CAM. For isoflurane anesthesia, the egg was exposed to an isoflurane concentration of 5% in oxygen. For induction, the eggs were placed into a narcosis induction chamber. Toxic side effects and only poor correlation between narcosis depth and dose limited the application of UC and Avertin and the authors clearly favored the use of Isoflurane due to its high tolerability enabling repeated imaging of the avian embryos at a daily basis. In 2013, Gebhardt et al. [70] applied a similar approach as Würbach et al. [71] to initially

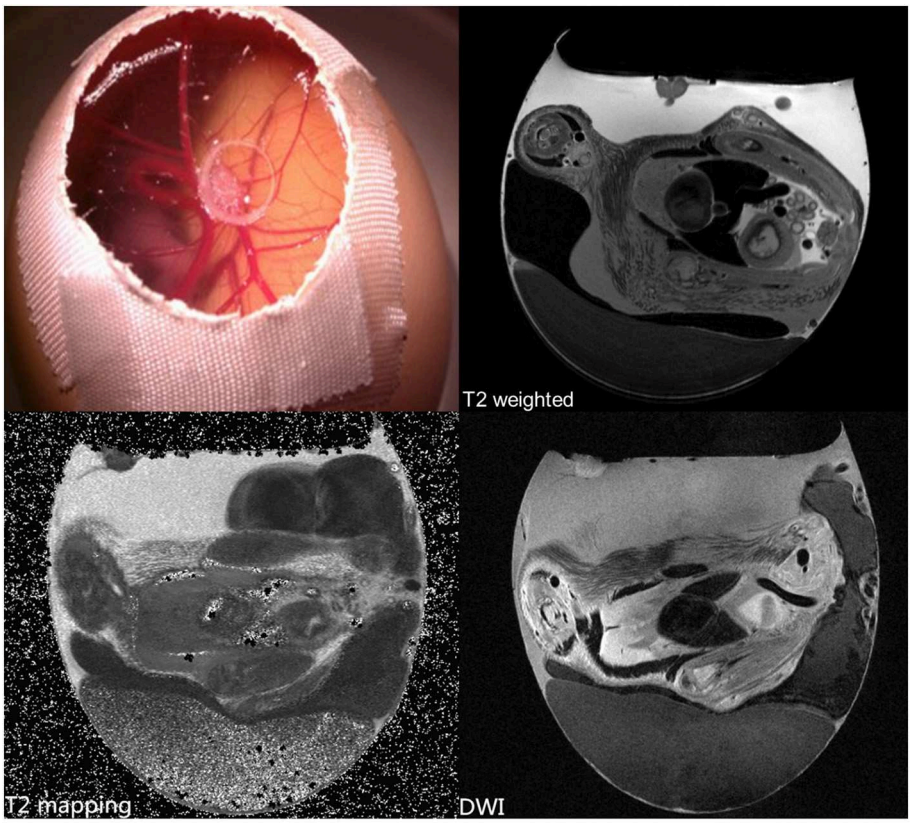

FIGURE 6 | *In vivo* high-resolution MRI with T2 and diffusion weighting (DWI), and T2 quantification of a Human breast tumor (carcinoma cell line MDA-MB-231) xenotransplanted on the CAM. Unpublished imaging material provided by Zuo obtained with precooling and MR protocols as described in [61].

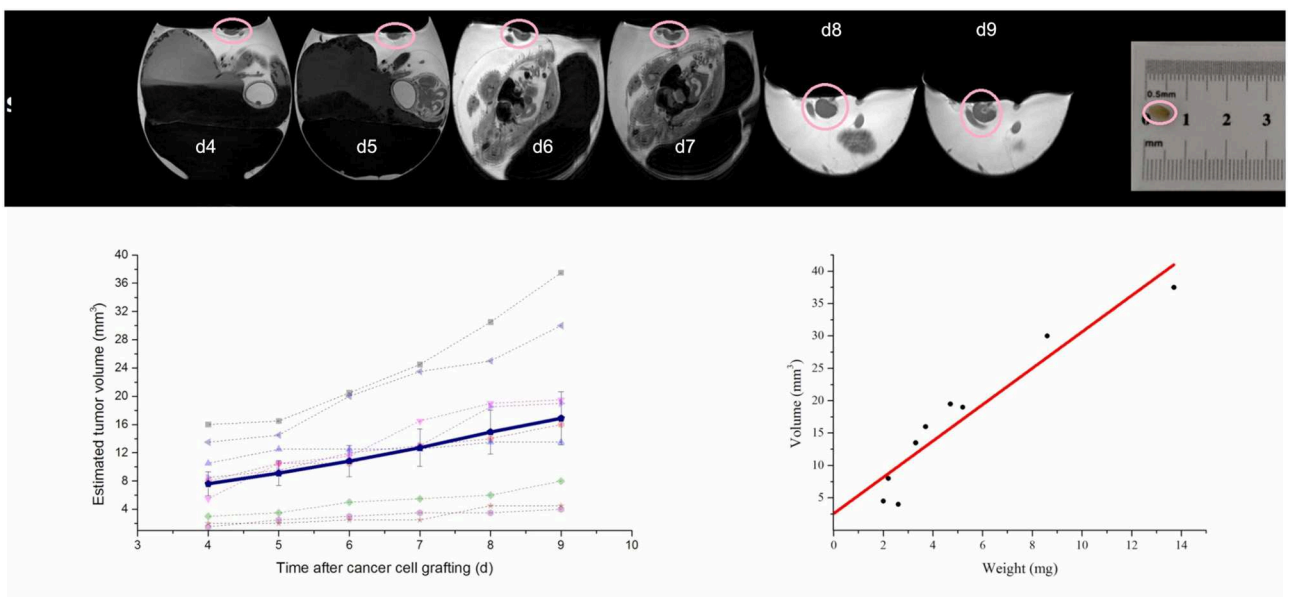

FIGURE 7 | Monitoring the progression of xenotransplanted tumor (circle) from day 4 to day 9 after cell seeding on the CAM. (Top) High-resolution T2 weighted MR images; (lower left) individual tumor volumes ($n = 9$) and mean volume progression (solid line); (lower right) correlation of tumor volume ($n = 9$) and weight after tumor resection at day 9. Modified from original research published in NMR Biomed: High-resolution MRI analysis of breast cancer xenograft on the chick chorioallantoic membrane. Zuo et al. [61].

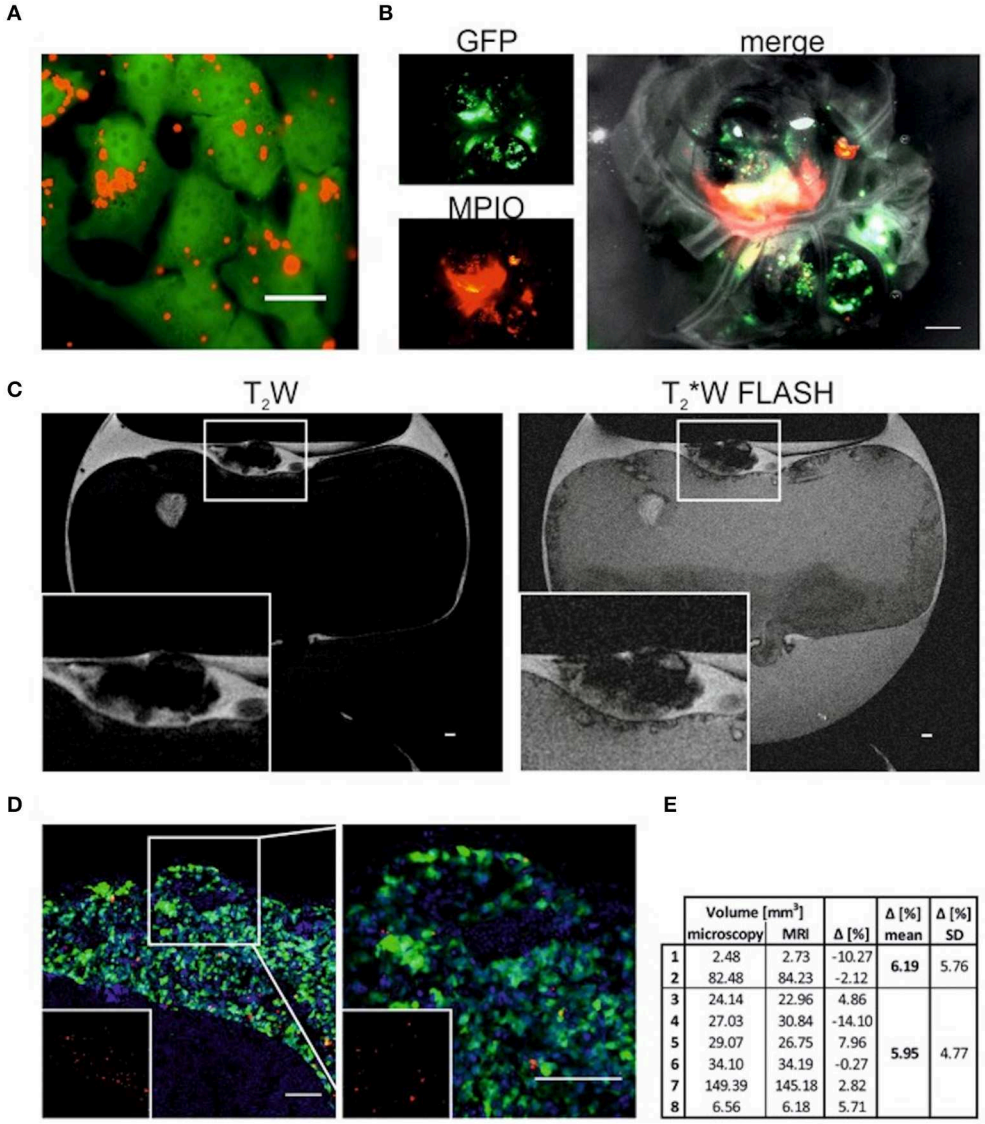

	Volume [mm³] microscopy	Volume [mm³] MRI	Δ [%]	Δ [%] mean	Δ [%] SD
1	2.48	2.73	-10.27	6.19	5.76
2	82.48	84.23	-2.12		
3	24.14	22.96	4.86	5.95	4.77
4	27.03	30.84	-14.10		
5	29.07	26.75	7.96		
6	34.10	34.19	-0.27		
7	149.39	145.18	2.82		
8	6.56	6.18	5.71		

FIGURE 8 | T2W and T2*W FLASH images of tumors labeled with MPIO **(A)** GFP-expressing SK-N-AS cells (green) 24 h -postlabeling with 20 mM MPIO (Suncoast Yellow Encapsulated Magnetic Polymers—Bangs Beads, Red). Scale bar is 20 mm. **(B)** Single channel and overlay image of neuroblastoma tumor postdissection formed by GFP-expressing SK-N-AS cells (green) which were labeled with MPIO (red) 48 h prior CAM implantation. Scale bar is 1000 mm. **(C)** Representative sagittal T2Wand T2*W FLASH MRI images of embryonated chicken egg at E14 **(A)**. Tumor formed by cells labeled with MPIO can be identified on top of the CAM (zoom in inset). Scale bar is 1000 mm. **(D)** Representative image of tumor formed on the CAM by GFP-expressing SK-N-AS cells (green) labeled with MPIO (red). Nuclei are stained with Hoechst (blue). Inset shows MPIO only (red). Right image is 2.5_ zoom. Scale bar is 100 mm. **(E)** Comparison of tumor volume (mm3) measured by microscopy or MRI. Tumors 1 to 2 were formed by cells without MPIO, tumors 3 to 8. This research was originally published under the terms of the CC BY license (Creative Commons Attribution 4.0 International License) in Mol Imaging: Magnetic Resonance Imaging for Characterization of a Chick Embryo Model of Cancer Cell Metastases. Herrmann et al. [58].

evaluate the dynamic behavior of new PET tracers in the chick embryo model as an *in vivo* assay. Various ^{18}F, ^{64}Cu, and ^{68}Ga-labeled compounds were investigated and the potential of the chick embryo model as efficient *in vivo* model could be shown.

Warnock et al. [69] demonstrated the use of the CAM for screening of novel PET tracers. At EDD 11, the eggs were opened and 5 x 10^6 human U87 glioblastoma cells in 20 μL of culture medium xenotransplanted onto the CAM. At EDD 18 PET/CT imaging of the tumors was performed. During scanning the egg was reproducible positioned in both systems in a small animal imaging cell (Minerve equipment veterenaire) allowing temperature control and isoflurane anesthesia (2% in air). Uptake of the radiotracer was clearly demonstrated by time-activity curves and in the PET images (**Figure 9**). Contrast-agent enhanced μCT data provided accurate anatomic correlation,

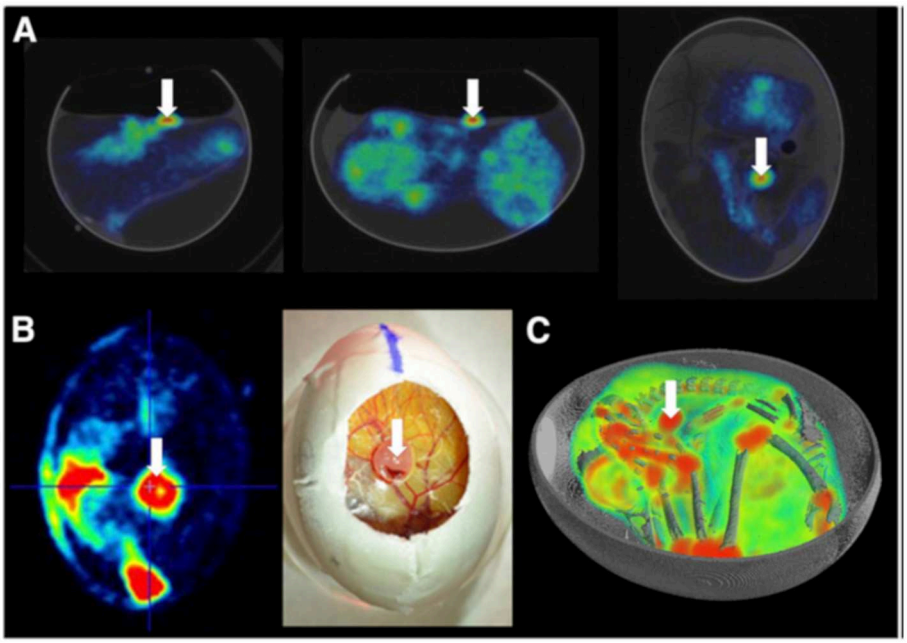

FIGURE 9 | (A) Two-dimensional coregistered PET and CT images of the chicken egg after [^{18}F]-FDG injection and 45 min tracer uptake. **(B)** Visual comparison of 18F-FDG uptake in glioblastoma at level of CAM to photograph illustrating tumor localization. **(C)** 3D visualization of overlaid PET and CT images for [^{18}F]-FDG uptake in embryo and U87 human glioblastoma tumor (white arrow). This research was originally published in JNM: *in vivo* PET/CT in a human glioblastoma chicken chorioallantoic membrane model: a new tool for oncology and radiotracer development. Warnock et al. © by the Society of Nuclear Medicine and Molecular Imaging, Inc. [69].

enabling distinction of the uptake in the joints and the tumor. Their outcome clearly indicated the potential of the suggested HET-CAM model for initial assessment of the pharmacokinetics of new compounds.

Haller et al. [19] investigated the tissue distribution and stability of different ^{18}F, ^{125}I, ^{99m}Tc, and ^{177}Lu—labeled radiopharmaceuticals. For imaging purposes the chick embryos were euthanized by shock-freezing in liquid nitrogen at different time points after administration of the radioactivity. In comparison with the established mouse models, they concluded a similar tissue distribution and stability of radiopharmaceuticals in the chick embryo. The very similar behavior in the two *in vivo* models indicate the potential of using the chick embryo as an inexpensive and simple test model for preclinical screening of novel radiopharmaceuticals. To overcome the limitations of the small anatomies with respective requirement of dedicated high-resolution imaging equipment, Freesmeyer et al. [108] suggested the translation of the work into ostrich eggs and demonstrated the potential use for different radiotracers even on conventional PET/CT systems. Even though overcoming the issues with small anatomy and high-spatial resolution requirements, ostrich eggs cannot be seen as a real alternative to chick embryos, since they are not readily available, hardly established in science, expensive and often do not fit into conventional small animal imaging equipment.

In a recent work of Zlatopolskiy et al. [68] the HET-CAM model was used for evaluation of radiotracers addressing the tryptophan metabolic pathway. An efficient method for the synthesis of fluorotryptophans, labeled in different positions with ^{18}F is presented and their biological evaluation regarding tumor targeting evaluated in the HET-CAM model. Therefor MCF7, PC-3, and NCI-H69 xenografts were cultivated on the CAM. The tissue distribution of the new agent 7-[^{18}F]FTrp in comparison to conventional ^{18}F^{-} was assessed after systemic injection. While in the ^{18}F-scans tracer uptake was mainly observed in bones, joints, and beak of the chick embryos, 7-[^{18}F]FTrp clearly delineated the tumor.

Even though CT represents an important imaging tool providing relevant anatomic information and has proven clinical success in combination with PET, its only limited soft tissue contrast is often insufficient. To that respect in 2019 Steinemann et al. [109] and Winter et al. [110] combined *in ovo* PET with MRI to make full advantage from the high sensitivity of PET and the excellent soft tissue contrast in MRI. Steinemann et al. used the imaging approach for monitoring the effectiveness of a new chimeric inhibitor (animacroxam, which combines histone deacetylase (HDAC) inhibitory and cytoskeleton-interfering pharmacophores) to the clinical approved HDAC in testicular germ cell tumor. Tumor plaques were grown from 10×10^6 2102EP cells mixed with 150 µl matrigel and transplanted onto the CAM. Imaging was performed three days after xenotransplantation to allow angiogenic connection of the xenograft to the CAM. Injection

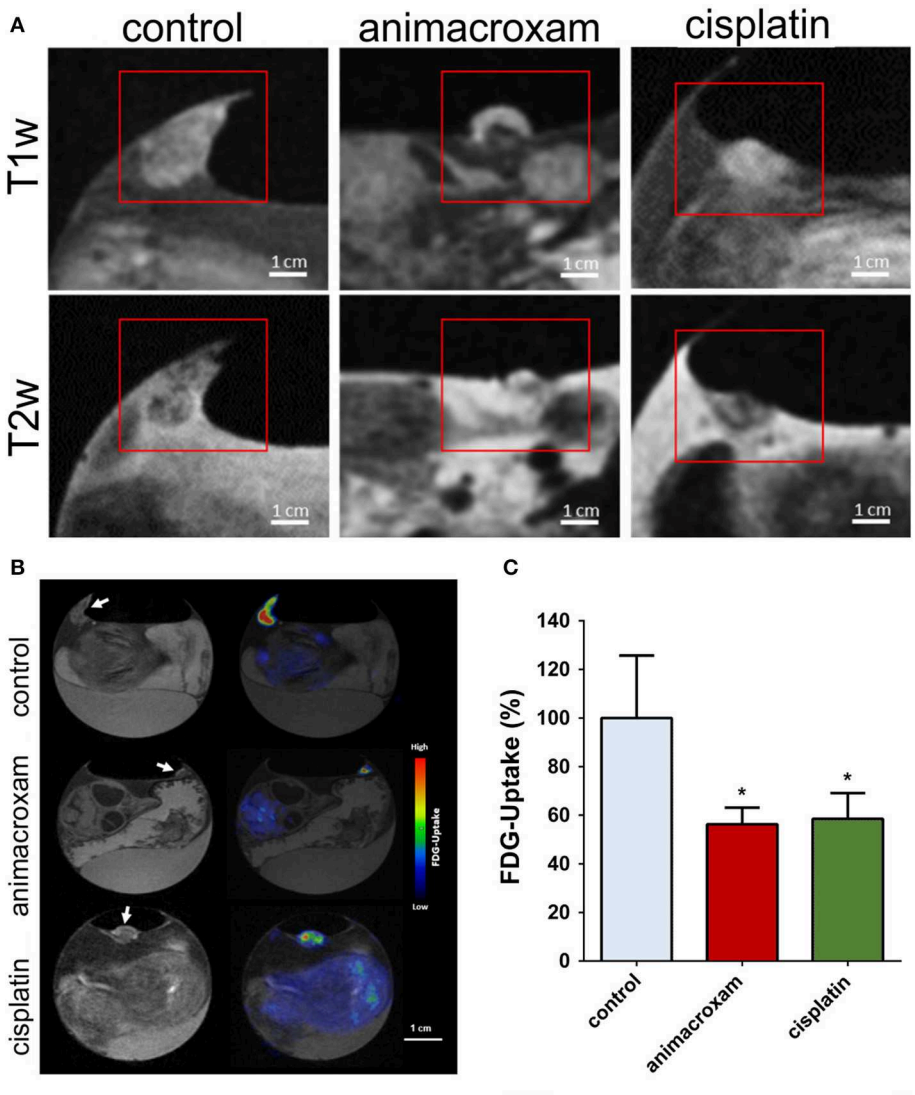

FIGURE 10 | Animacroxam induces 'cap formation' and suppresses glucose uptake in inoculated TGCT plaques. **(A)** T1w and T2w images of control-, animacroxam-, and cisplatin-treated tumor plaques. Animacroxam-treated tumors show a distinct viable tumor core (dark in T1w-/bright in T2w images) and a necrotic cap (bright in T1w-/dark in T2w images). **(B)** T1w and corresponding PET-MR images of [^{18}F]-FDG uptake in tumor plaques treated with NaCl, animacroxam, or cisplatin. **(C)** Animacroxam (5.0 μm)- and cisplatin (2.5 μm)-treated tumor plaques showed a reduced uptake of [^{18}F]-FDG. Results are shown as means ± SEM of at least $n = 3$ independent experiments. Scale bar = 1 cm. *P-values of ≤ 0.05, unpaired t-test. This research was originally published under the terms of the Creative Commons Attribution License (CC BY) in Molecular Oncology: Antitumor and antiangiogenic activity of the novel chimeric inhibitor animacroxam in testicular germ cell cancer, Steinemann et al. [109].

of the compounds [concentrations calculated assuming 1 mL blood volume: 5 μM animacroxam, 2.5 μM cisplatin, or NaCl (0.9%)], was done intravenously via a 30G syringe. The tumor volume was derived from MRI measurements (3D T1w-GRE, 290 x 290 x 500 μm^3, TR/TE = 50 ms/2.7 ms; 2D RARE, 290 x 290 x 700 μm^3, TR/TE = 8885 ms/100 ms) prior and 7 days after treatment. Immobilization of the chick embryos was obtained by 1 h precooling. Tumors could be clearly delineated in the MRI data and respective volumes quantified. Respective glucose uptake of the tumors was assessed by [^{18}F]-FDG PET imaging (0.1 mL of 12 MBq). Fusion of the PET and MRI data showed excellent agreement between tumor extend and FDG uptake (**Figure 10**). The observed reduction in tumor volume under treatment correlated well with the observed reduced glucose uptake. Winter et al. evaluated the HET-CAM for initial testing of the binding specificity of targeted compounds. They used the well-characterized PSMA-specific PET radiotracer [^{68}Ga]-PSMA-11 to demonstrate the principle of the HET-CAM model for evaluation of specific radioligand accumulation in prostate cancer xenografts (**Figure 11**). At EDD 6, tumor cells of the PSMA-positive cell line LNCaP C4-2 (1 x 10^6 cells) and the PSMA-negative control PC-3 (7.5 x 10^5

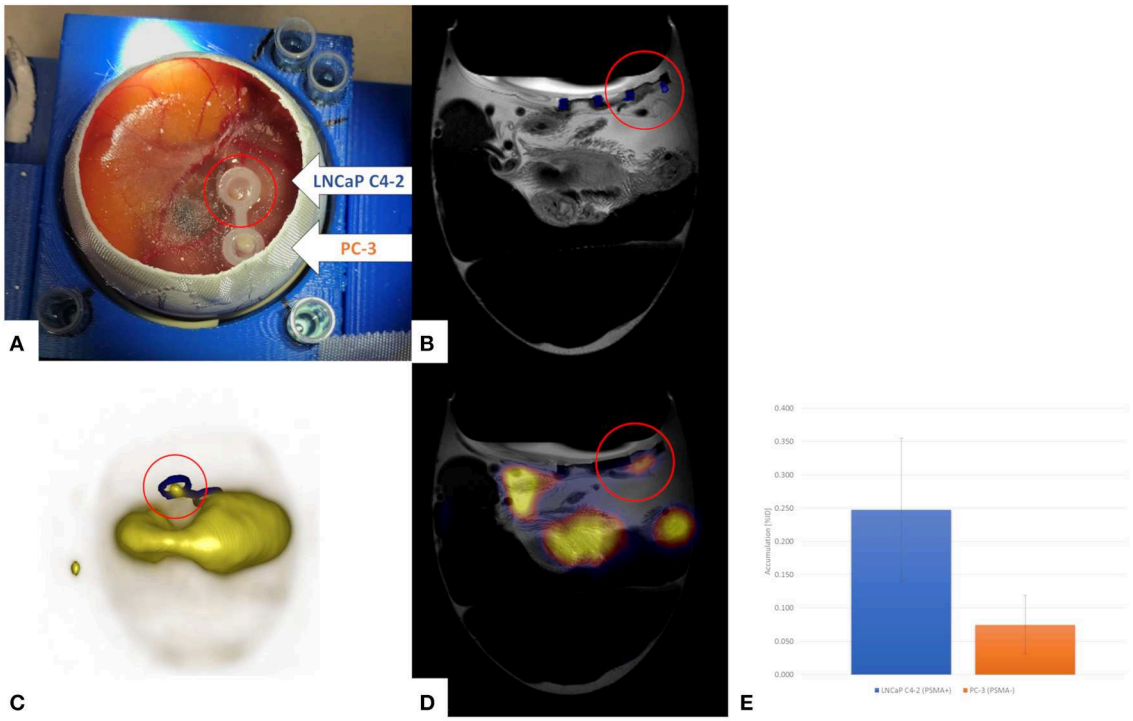

FIGURE 11 | PET/MRI for quantification of the PSMA-specific PET radiotracer [^{68}Ga]-PSMA-11 in the HET-CAM model with dual tumor seeding (LNCaP C4-2, PSMAQ17 positive; PC-3, PSMA negative) **(A)**. The tumors can be nicely visualized by high-resolution MRI (**B**, red circle). Distribution of the [^{68}Ga]-PSMA-11 by PET reveals strong signal at one location of the CAM and some general accumulation in the chick embryo **(C)**. Fusion of the PET and MRI data **(D)** reveals tracer accumulation in the PSMA positive tumor (red circle), which is proven by gamma counting after resection of the tumors **(E)**. Unpublished imaging material provided by Winter G. and Li H.

cells) mixed in Matrigel (40%, v/v) were grafted on the CAM in two silicon rings. MR and PET imaging was performed starting on EDD 12. Anatomical information was provided by high-resolution imaging using a small animal MR based on the protocol of Zuo et al. [61, 65]. For PET, 150 µl of [^{68}Ga]-PSMA-11 solution was injected into a chorioallantoic membrane vessel followed by a dynamic 60 minutes PET scan. Registration between both imaging modalities was achieved by a self-built animal holder with PET and MRI visible fiducial markers. Tumor growth could be quantified by MR imaging. In addition to PET imaging the tumor entities were excised from the membrane after measurement and the accumulated activity was separately quantified by γ-counter (COBRA II, Perkin Elmer) detection. As expected, in comparison to the PC-3 tumors, higher accumulation of [^{68}Ga]-PSMA-11 was observed in the LNCaP C4-2 tumors, indicating the applicability of the HET-CAM model for initial testing of binding specificity of targeted compounds.

DISCUSSION

The HET-CAM model has been exerted to numerous applications. It represents a simple, quick, and low-cost model, not rising any regulatory concerns in many countries if sacrificed before hatching. However, there is a consensus in the scientific community that it is illogical to conclude that the neural capacity to experience pain is not fully developed prior to hatching and that beyond a critical point in development avian embryos are capable of experiencing pain. The exact stage of development at which this capacity is sufficiently developed to warrant concern has not yet been determined. Society recognizes that a critical period in chick embryo development occurs 72 h prior to hatching and from an ethical point of view embryos should be sacrificed prior to EDD 18.

Since the HET-CAM model represents a naturally immunodeficient host, xenotransplantation of many kinds of tumors without species-specific limitations are possible. Even considering the fact that not all organs are fully developed, the established circulation and the highly vascularized CAM, which is connected to the embryo through a continuous circulatory system make it a natural candidate in-between cell culture and animal experiments, especially for initial testing of new compounds. Even though not finally established, it will likely play an important role in early drug development as pointed out in **Figure 12**. Compounds without detectable toxicity in cell and eventually zebra fish assays, may be initially evaluated regarding efficacy and biodistribution in the HET-CAM model, thereby reinforcing the potential of this convenient, 3R compliant, *in vivo*

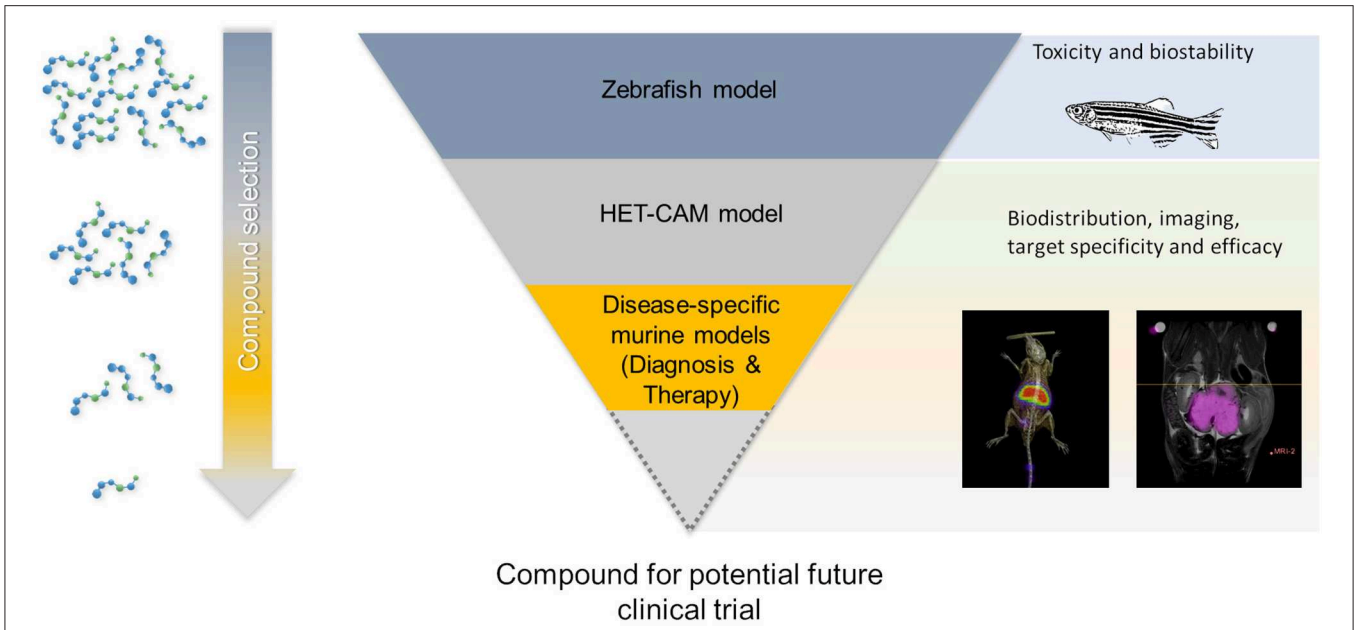

FIGURE 12 | Potential role of PET-MRI imaging in the HET-CAM model within new drug developments.

model for cancer research. Only compounds showing promising properties will then further be evaluated in animal models, thus reducing the need for animal studies and related costs.

Non-invasive imaging will likely play an increasingly important role for direct visualization of the biodistribution of respectively labeled compounds and longitudinal monitoring of surrogate markers such as tumor progression and metabolism. MRI appears as an attractive imaging approach providing flexible image contrast and assessment to different tissue-specific parameters like MR relaxation times, diffusion and perfusion. Even though it offers the possibility of tailoring image contrast to the specific application, its intrinsic low sensitivity often limits its application in identification of small amounts or only traces of compounds. This limitation raises the increasing interest in using PET in the context of HET-CAM imaging. The excellent sensitivity of PET combined with the excellent anatomic detail of MRI appears as an ideal combination for anatomic, metabolic, and molecular imaging in the HET-CAM model.

Even though in PET motion compensation of the embryo may not be of paramount importance due to its only limited spatial resolution, in MRI coping with embryo motion is one of the major challenges to finally achieve the required high-spatial resolution. Over the last years efficient immobilization approaches of the chick embryo have successfully been evaluated *in ovo* (**Table 1**). Promising approaches include the precooling of the egg prior to scanning, the application of halothane and isoflurane, and the use of anesthesia agents dropped directly onto the CAM. Good to excellent immobilization could be achieved with almost all approaches. Major differences were reported regarding immobilization duration and resulting possible image acquisition times, tolerability by the chick embryo, side effects, and easiness to use. For high-resolution anatomic imaging, precooling appears as an excellent approach, allowing long scan times of up to one hour and being easy-to-use. However, the related slowdown in metabolism [113] and blood flow [58] may limit its application in cases where physiological properties are under investigation. Here, in contrast to halothane, isoflurane was reported to not impact aortic blood flow and cardiac performance [114] and may be a good alternative with the limitation of a quite complex imaging setup. Both approaches are well tolerated by the chick embryo allowing for repeated measurements in longitudinal studies. Liquid anesthetics applied by directly dropping onto the CAM are easy to use and a variety of agents have been reported with widely varying anesthesia efficiency and often toxic side effects [58, 106, 107]. Even though, ketamine was reported to reduce cardiac contraction force in isolated chick embryo heart at EDD 4 and EDD 7 [115], Herrmann et al. reported the advantage of ketamine over precooling for time-of-flight MRI [58] and showed its possible use in applications being sensitive compromised circulation or metabolism in cases of rather short acquisition times.

This review specifically addresses MRI/PET imaging techniques for HET-CAM applications. Even though highly attractive for high-quality multi-contrast morphological and functional imaging in combination with high-sensitive imaging of radio-labeled compounds, both represent high-cost imaging techniques requiring long acquisition times with only limited applicability to high-throughput applications. A wide range of alternative somehow competing techniques have been proposed over recent years. Most prominent to mention at this point are

TABLE 1 | Overview of reported *in vivo* in ovo imaging and spectroscopy studies.

References	Modality	Application	Imaging technique	Dimension	Spatial resolution	Immobilization	EDD	Scan time
Bone et al. [81]	MRI (1H, 1.5T)	Embryonic anatomy	T1-/T2-weighted SE	3D	200 × 200 × 1200 μm^3	Precooling (EDD 11 20 minutes, EDD15 90 minutes) on ice chips	11, 15	Not reported
Effmann et al. [83]	MRI (1H, 2T)	Embryonic anatomy	T1-weighted SE	2D	50 × 50 × 600 μm^3	Not reported	4,6,9	1–2 h
Moseley et al. [54]	MRS (31P, 2T), MRI (1H, 2T)	Metabolic (MRS) and anatomic (MRI) development	T1/T2-weighted SE	Single voxel (MRS), 2D (MRI)	Whole egg (MRS) 270 × 270 × 2000 μm^3 to 350 × 700 × 3000 μm^3 (MRI)	Not reported	4, 9, 12, 15, 17, 18, 19, 20, 21 (MRS), 5, 9, 15, 23 (MRI)	20 min (512 NSA, MRS), not reported (MRI)
Lirette et al. [85]	MRS (31P, 1H, 2T)	Metabolic development, fat-water fraction		Single voxel	Whole egg	Halothane	0, 2, 4, 6, 8, 10, 12, 14, 16, 17, 19, 20	
Peebles et al. [86]	MRS (1H, 7T), MRI (1H, 7T)	Metabolic (MRS) and diffusion (MRI) response to hypoxia and recovery	PRESS, 2pt diffusion	Single voxel (MRS), 2D (MRI)	6 × 6 × 6 mm^3 (MRS), 230 × 460 × 2000 μm^3 (MRI)	Ketamine	19	21.3 min (MRS), not reported (MRI)
Falen et al. [53]	MRI (1H, 2T)	Yolk structure	SE	2D	250 × 250 × 1250 μm^3 to 500 × 500 × 1250 μm^3	Not reported	daily	1 h
Hutchison et al. [87]	MRI (1H, 2T)	Yolk structure	T1-/T2-weighted SE	2D	235 × 310 μm^2	Not reported	1	Not reported
Donoghue et al. [88]	MRI (1H, 1.5T)	Residue transfer	IR-FLASH (MP-RAGE)	3D	1000 × 780 × 1250 μm^3	Precooling	not reported	Not reported
Holmes et al. [93]	MRI (1H, 7T)	Cardiac function	T1–weighted GE	2D	300 × 300 × 1500 μm^3	Self-gated	8, 13, 16, 20	Not reported
Bain et al. [51]	MRI (1H, 7T)	Chick embryo development	T2–weighted SE	2D	192 × 195 × 500 μm^3	Precooling	12, 15, 17, 18, 19, 20	25 min
Boss et al. [50]	MRI (1H, 7T)	MR relaxation parameter changes during embryonic development	IR–TSE (T1–mapping), HASTE (T2–mapping), MT- prepared GE	2D (T1/T2– mapping), 3D (MTR)	180 × 180 × 1000 μm^3 (T1–mapping), 260 × 260 × 1000 μm^3(HASTE), 230 × 230 × 1000 μm^3 (MTR)	Ketamine	5, 8, 11, 16	Not reported
Zhou et al. [111]	MRI (1H, 3T)	Muscle fiber tracking during embryonic development	T1- / T2- weighted TSE, DTI	2D	200 × 200 × 2000 μm^3 (T1w), 200 × 200 × 1200 μm^3 (T2w), 600 × 600 × 1200 μm^3 (dti)	No, single- and double-precooling	4, 5, 6,7, 8, 9, 10, 11, 12, 13, 18, 19	2 min 17 s (T1w), 12 min 23 s (t2w), 31 min 14 s (DTI)
Lindner et al. [48]	MRI (1H, 7T)	Embryonic development of the eye	T2–weighted TSE	2D	74 × 74 × 700 μm^3	Bedding on crushed ice for EDD > 10	1–20 daily	
Dingman et al. [112]	MRI (19F, not reported)	Biodistribution of 19F-labeled compound	Not-reported	Not-reported	Not-reported	Not-reported	15, 16, 17, 18	
Oppitz et al. [98]	MRI (1H, 3T)	Migration of iron labeled melanoma cells	T2*-weighted	3D	300^3–1000^3 μm^3	Not reported	6, 9, 18, 20	12 s / slice

(Continued)

TABLE 1 | Continued

References	Modality	Application	Imaging technique	Dimension	Spatial resolution	Immobilization	EDD	Scan time
Faucher et al. [100]	MRI (1H, 1.5T)	Localization of Gd—labeled GL-261 glioblastoma cells	T1–weighted GR	3D	350 × 350 × 500 μm^3	Precooling	10, 11, 13	6–7 min
Zuo et al. [61]	MRI (1H, 11.7T)	CAM tumor morphology	T2–weighted TSE, T2 mapping, diffusion weighted, T1–weighted GE	2D (T2, T2–mapping, DWI) 3D (T1 weighted GE)	77 × 91 × 500 μm^3 (t2w), 200 × 200 × 500 μm^3 (DWI), 104 × 98 × 500 μm^3 (T2 mapping), 100 × 100 × 560 μm^3	Precooling	11–16, daily	15 min 32s (t2w), 60 min (DWI), 34 min (T2 mapping), 4 min 9 s (t1w)
Zuo et al. [65]	MRI (1H, 11.7T)	Biodistribution of Gd–labeled compounds	T1-weighted GE, T2-weighted SE	3D (T1w), 2D (T1w)	100 × 100 × 560 μm (T1w), 77 × 91 × 500 μm^3 (t2w)	Precooling	16 (injection), pre- and 30 min, 3 h, 20 h, 40 h after injection	4 min 9 s (T1w), 15 min 32 s (t2w)
Pfiffner et al. [105]	MRI (1H, 4.7T)	Perfusion capacity of 3D biomaterials	T1-weighted GE, T1-/T2-mapping	2D	500 × 500 × 1000 μm^3	Ketamine	14	25 s (GE), 9 min 40 s (mapping)
Waschkies et al. [106]	see Pfiffner et al. [105]	See Pfiffner et al. [105]	See Pfiffner et al. [105]	See Pfiffner et al. [105]	See Pfiffner et al. [105]	Metetomidone, thiopental, ketamine/midazolam	see Pfiffner et al. [105]	See Pfiffner et al. [105]
Herrmann et al. [58]	MRI(1H, 9.4T)	Tracking of magnetic particle labeled tumor cells	T2-weighted TSE, T2*-weighted GE, Time of flight (TOF)	2D	88/166 × 88/166 × 400/500 mm3 (t2w), 88 × 88 × 400 μm^3 (t2*, tof)	Precooling (T2-/T2*w), ketamine (Tof)	14	13 min 24 s–31 min 56 s (t2w), 22 min 35s (T2*), 12 min 4 s (Tof)
Würbach et al. [71]	PET (^{18}F)	Bone metabolism	Static, dynamic	3D	400 × 400 × 800 μm^3	Isoflurane	13–18	75 min
Heidrich et al. [107]	PET/μCT	Immobilization	Static	3D	Not reported	Isoflurane, 2,2,2-tribromoethanol, urethane/α-chloralose	11–18	6 min
Warnock et al. [69]	PET (^{18}F) / μCT	Screening of novel PET tracer	Dynamic, static	3D	433 × 433 × 796 μm^3 (PET), 100^3 μm^3 (μct)	Isoflurane	18	45 min (PET), not-reported (μct)
Zlatopolskiy et al. [68]	PET (^{18}F)	Tracer accumulation in CAM tumor	Static	3D	1.4^3 mm^3 (PET)	Isoflurane	7	30 min
Steinemann et al. [109]	PET (^{18}F) / MRI (1H, 1T)	Tumor growth and metabolism	T1-weighted GE, T2-weighted TSE, static (PET)	3D (GE, PET), 2D (TSE)	290 × 290 × 500 μm^3 (GE), 290 × 290 × 700 μm^3 (TSE), not reported (PET)	Precooling	10, 17	Not reported
Winter et al. [110]	PET (^{68}Ga), MRI (1H, 11.7T)	Binding specificity of target-specific radioligands	Dynamic (PET), T2-/T1–weighted SE (MRI)	3D (PET), 2D (MRI)	1.4^3 mm^3 (PET), 100 × 100 × 560 μm (T1w), 77 × 91 × 500 μm^3 (t2w)	Precooling (MRI), none (PET)	12	

MRI, magnetic resonance imaging; MRS, magnetic resonance spectroscopy; PET, positron emission tomography; μCT, microscopy computer tomography; SE, spin echo; TSE, turbo spin echo; GE, gradient echo; IR, inversion recovery; MT, magnetization transfer; FLASH, fast low angle shot; HASTE, half-Fourier single-shot turbo spin echo.

optical methods [116, 117] including bioluminescence [118], fluorescence [119], and tomographic [120, 121] techniques. Furthermore, ultrasonographic imaging [122], x-ray based tomographic [45] and even photoacoustic techniques [123] have been introduced, the latter of which with the potential for label-free imaging. In combination with single photon emission tomography (SPECT), tomographic x-ray techniques have been applied to initial evaluation of radiopharmaceuticals in chick embryos [19].

In conclusion, the expected increasing interest in the HET-CAM model as an intermediate step between cell culture and animal model for initial testing of new compounds makes *in ovo* imaging an important tool for monitoring the fate of compounds after systemic injection or surrogate markers. The combination of MRI and PET appears promising by combining the sensitivity of PET with detailed anatomic and functional information provided by MRI.

AUTHOR CONTRIBUTIONS

GW, AK, JL, AA, AB, HL, and ZZ performed measurements in the context of the presented work. FJ and ML provided in-depth knowledge on nano-particles. GW and VR wrote the manuscript, and are responsible for the in ovo experiments.

ACKNOWLEDGMENTS

The authors received funding from the European Union's Horizon 2020 research and innovation programme under grant agreement No. 667192, and by the Deutsche Forschungsgemeinschaft (DFG) through the Collaborative Research Center 1279—The exploration of the Human Peptidome. Further the general support of the MoMAN imaging center of Ulm University is acknowledged.

REFERENCES

1. Ribatti D. The chick embryo chorioallantoic membrane (CAM). A multifaceted experimental model. *Mech Dev.* (2016) **141**:70–7. doi: 10.1016/j.mod.2016.05.003
2. Buchele B, Zugmaier W, Genze F, Simmet T. High-performance liquid chromatographic determination of acetyl-11-keto-alpha-boswellic acid, a novel pentacyclic triterpenoid, in plasma using a fluorinated stationary phase and photodiode array detection: application in pharmacokinetic studies. *J Chromatogr B Analyt Technol Biomed Life Sci.* (2005) **829**:144–8. doi: 10.1016/j.jchromb.2005.09.043
3. Syrovets T, Gschwend JE, Buchele B, Laumonnier Y, Zugmaier W, Genze F, et al. Inhibition of IkappaB kinase activity by acetyl-boswellic acids promotes apoptosis in androgen-independent PC-3 prostate cancer cells in vitro and in vivo. *J Biol Chem.* (2005) **280**:6170–80. doi: 10.1074/jbc.M409477200
4. Estrada AC, Syrovets T, Pitterle K, Lunov O, Buchele B, Schimana-Pfeifer J, et al. Tirucallic acids are novel pleckstrin homology domain-dependent Akt inhibitors inducing apoptosis in prostate cancer cells. *Mol Pharmacol.* (2010) **77**:378–87. doi: 10.1124/mol.109.060475
5. Morad SA, Schmidt C, Buchele B, Schneider B, Wenzler M, Syrovets T, et al. (8R)-3beta,8-dihydroxypolypoda-13E,17E,21-triene induces cell cycle arrest and apoptosis in treatment-resistant prostate cancer cells. *J Nat Prod.* (2011) **74**:1731–6. doi: 10.1021/np200161a
6. Morad SA, Schmid M, Buchele B, Siehl HU, El Gafaary M, Lunov O, et al. A novel semisynthetic inhibitor of the FRB domain of mammalian target of rapamycin blocks proliferation and triggers apoptosis in chemoresistant prostate cancer cells. *Mol Pharmacol.* (2013) **83**:531–41. doi: 10.1124/mol.112.081349
7. Vogler M, Walczak H, Stadel D, Haas TL, Genze F, Jovanovic M, et al. Targeting XIAP bypasses Bcl-2-mediated resistance to TRAIL and cooperates with TRAIL to suppress pancreatic cancer growth in vitro and in vivo. *Cancer Res.* (2008) **68**:7956–65. doi: 10.1158/0008-5472.CAN-08-1296
8. Swadi RR, Sampat K, Herrmann A, Losty PD, See V, Moss DJ. CDK inhibitors reduce cell proliferation and reverse hypoxia-induced metastasis of neuroblastoma tumours in a chick embryo model. *Sci Rep.* (2019) **9**:9136. doi: 10.1038/s41598-019-45571-8
9. Loos C, Syrovets T, Musyanovych A, Mailander V, Landfester K, Simmet T. Amino-functionalized nanoparticles as inhibitors of mTOR and inducers of cell cycle arrest in leukemia cells. *Biomaterials.* (2014) **35**:1944–53. doi: 10.1016/j.biomaterials.2013.11.056
10. Vargas A, Zeisser-Labouebe M, Lange N, Gurny R, Delie F. The chick embryo and its chorioallantoic membrane (CAM) for the in vivo evaluation of drug delivery systems. *Adv Drug Deliv Rev.* (2007) **59**:1162–76. doi: 10.1016/j.addr.2007.04.019
11. Lunov O, Syrovets T, Loos C, Beil J, Delacher M, Tron K, et al. Differential uptake of functionalized polystyrene nanoparticles by human macrophages and a monocytic cell line. *ACS Nano.* (2011) **5**:1657–69. doi: 10.1021/nn2000756
12. Leng T, Miller JM, Bilbao KV, Palanker DV, Huie P, Blumenkranz MS. The chick chorioallantoic membrane as a model tissue for surgical retinal research and simulation. *Retina.* (2004) **24**:427–34. doi: 10.1097/00006982-200406000-00014
13. DeBord LC, Pathak RR, Villaneuva M, Liu HC, Harrington DA, Yu W, et al. The chick chorioallantoic membrane (CAM) as a versatile patient-derived xenograft (PDX) platform for precision medicine and preclinical research. *Am J Cancer Res.* (2018) **8**:1642–60.
14. Vu BT, Shahin SA, Croissant J, Fatieiev Y, Matsumoto K, Le-Hoang Doan T, et al. Chick chorioallantoic membrane assay as an in vivo model to study the effect of nanoparticle-based anticancer drugs in ovarian cancer. *Sci Rep.* (2018) **8**:8524. doi: 10.1038/s41598-018-25573-8
15. Ribatti D, Tamma R. The chick embryo chorioallantoic membrane as an in vivo experimental model to study human neuroblastoma. *J Cell Physiol.* (2018) **234**:152–7. doi: 10.1002/jcp.26773
16. Ribatti D. The chick embryo chorioallantoic membrane as a model for tumor biology. *Exp Cell Res.* (2014) **328**:314–24. doi: 10.1016/j.yexcr.2014.06.010
17. Gabrielli MG, Accili D. The chick chorioallantoic membrane: a model of molecular, structural, and functional adaptation to transepithelial ion transport and barrier function during embryonic development. *J Biomed Biotechnol.* (2010) 2010:940741. doi: 10.1155/2010/940741
18. Nowak-Sliwinska P, Segura T, Iruela-Arispe ML. The chicken chorioallantoic membrane model in biology, medicine and bioengineering. *Angiogenesis.* (2014) **17**:779–804. doi: 10.1007/s10456-014-9440-7
19. Haller S, Ametamey SM, Schibli R, Muller C. Investigation of the chick embryo as a potential alternative to the mouse for evaluation of radiopharmaceuticals. *Nucl Med Biol.* (2015) **42**:226–33. doi: 10.1016/j.nucmedbio.2014.10.010
20. Duman R, Ertekin T, Duman R, Aslan E, Sabaner MC, Cetinkaya E. The novel model: Experimental optical coherence tomography-guided anterior segment imaging chick embryo model. *Indian J Ophthalmol.* (2019) **67**:54–8. doi: 10.4103/ijo.IJO_263_18
21. Ko ZY, Mehta K, Jamil M, Yap CH, Chen N. A method to study the hemodynamics of chicken embryo's aortic arches using optical coherence tomography. *J Biophotonics.* (2017) **10**:353–9. doi: 10.1002/jbio.201600119
22. Goenezen S, Chivukula VK, Midgett M, Phan L, Rugonyi S. 4D subject-specific inverse modeling of the chick embryonic heart outflow tract hemodynamics. *Biomech Model Mechanobiol.* (2016) **15**:723–43. doi: 10.1007/s10237-015-0720-y

23. Midgett M, Chivukula VK, Dorn C, Wallace S, Rugonyi S. Blood flow through the embryonic heart outflow tract during cardiac looping in HH13-HH18 chicken embryos. *J R Soc Interface.* (2015) **12**:20150652. doi: 10.1098/rsif.2015.0652
24. Ma Z, Dou S, Zhao Y, Guo C, Liu J, Wang Q, et al. In vivo assessment of wall strain in embryonic chick heart by spectral domain optical coherence tomography. *Appl Opt.* (2015) **54**:9253–7. doi: 10.1364/AO.54.009253
25. Filas BA, Xu G, Taber LA. Probing regional mechanical properties of embryonic tissue using microindentation and optical coherence tomography. *Methods Mol Biol.* (2015) **1189**:3–16. doi: 10.1007/978-1-4939-1164-6_1
26. Yin X, Liu A, Thornburg KL, Wang RK, Rugonyi S. Extracting cardiac shapes and motion of the chick embryo heart outflow tract from four-dimensional optical coherence tomography images. *J Biomed Opt.* (2012) **17**:96005–1. doi: 10.1117/1.JBO.17.9.096005
27. Liu A, Yin X, Shi L, Li P, Thornburg KL, Wang R, et al. Biomechanics of the chick embryonic heart outflow tract at HH18 using 4D optical coherence tomography imaging and computational modeling. *PLoS ONE.* (2012) **7**:e40869. doi: 10.1371/journal.pone.0040869
28. Li P, Wang RK. Optical coherence tomography provides an ability to assess mechanical property of cardiac wall of developing outflow tract in embryonic heart in vivo. *J Biomed Opt.* (2012) **17**:120502. doi: 10.1117/1.JBO.17.12.120502
29. Li P, Yin X, Shi L, Rugonyi S, Wang RK. In vivo functional imaging of blood flow and wall strain rate in outflow tract of embryonic chick heart using ultrafast spectral domain optical coherence tomography. *J Biomed Opt.* (2012) **17**:96006–1. doi: 10.1117/1.JBO.17.9.096006
30. Happel CM, Thommes J, Thrane L, Manner J, Ortmaier T, Heimann B, et al. Rotationally acquired four-dimensional optical coherence tomography of embryonic chick hearts using retrospective gating on the common central A-scan. *J Biomed Opt.* (2011) **16**:096007. doi: 10.1117/1.3622491
31. Liu X, Zhang K, Huang Y, Kang JU. Spectroscopic-speckle variance OCT for microvasculature detection and analysis. *Biomed Opt Express.* (2011) **2**:2995–3009. doi: 10.1364/BOE.2.002995
32. Li P, Yin X, Shi L, Liu A, Rugonyi S, Wang R. Measurement of strain and strain rate in embryonic chick heart in vivo using spectral domain optical coherence tomography. *IEEE Trans Biomed Eng.* (2011) **58**:51. doi: 10.1109/TBME.2011.2153851
33. Osiac E, Saftoiu A, Gheonea DI, Mandrila I, Angelescu R. Optical coherence tomography and Doppler optical coherence tomography in the gastrointestinal tract. *World J Gastroenterol.* (2011) **17**:15–20. doi: 10.3748/wjg.v17.i1.15
34. Manner J, Thrane L, Norozi K, Yelbuz TM. In vivo imaging of the cyclic changes in cross-sectional shape of the ventricular segment of pulsating embryonic chick hearts at stages 14 to 17: a contribution to the understanding of the ontogenesis of cardiac pumping function. *Dev Dyn.* (2009) **238**:3273–84. doi: 10.1002/dvdy.22159
35. Liu A, Wang R, Thornburg KL, Rugonyi S. Efficient postacquisition synchronization of 4-D nongated cardiac images obtained from optical coherence tomography: application to 4-D reconstruction of the chick embryonic heart. *J Biomed Opt.* (2009) **14**:044020. doi: 10.1117/1.3184462
36. Rugonyi S, Shaut C, Liu A, Thornburg K, Wang RK. Changes in wall motion and blood flow in the outflow tract of chick embryonic hearts observed with optical coherence tomography after outflow tract banding and vitelline-vein ligation. *Phys Med Biol.* (2008) **53**:5077–91. doi: 10.1088/0031-9155/53/18/015
37. Filas BA, Knutsen AK, Bayly PV, Taber LA. A new method for measuring deformation of folding surfaces during morphogenesis. *J Biomech Eng.* (2008) **130**:061010. doi: 10.1115/1.2979866
38. Chen Z, Milner TE, Srinivas S, Wang X, Malekafzali A, van Gemert MJ, et al. Noninvasive imaging of in vivo blood flow velocity using optical Doppler tomography. *Opt Lett.* (1997) **22**:1119–21. doi: 10.1364/OL.22.001119
39. Seal HE, Lilian SJ, Popratiloff A, Hirsch JC, Peusner KD. Implementing the chick embryo model to study vestibular developmental disorders. *J Neurophysiol.* (2019) **122**:2272–83. doi: 10.1152/jn.00434.2019
40. Shigeta Y, Fujiwara N, Koike M, Yamataka A, Doi T. Bone mineral density is increased in the cadmium-induced omphalocele chick model by using three-dimensional micro-computed tomography. *Pediatr Surg Int.* (2019) **35**:911–4. doi: 10.1007/s00383-019-04501-5
41. Moreno-Jimenez I, Hulsart-Billstrom G, Lanham SA, Janeczek AA, Kontouli N, Kanczler JM, et al. The chorioallantoic membrane (CAM) assay for the study of human bone regeneration: a refinement animal model for tissue engineering. *Sci Rep.* (2016) **6**:32168. doi: 10.1038/srep32168
42. Yair R, Shahar R, Uni Z. In ovo feeding with minerals and vitamin D3 improves bone properties in hatchlings and mature broilers. *Poult Sci.* (2015) **94**:2695–707. doi: 10.3382/ps/pev252
43. Milisits G, Donko T, Dalle Zotte A, Sartori A, Szentirmai E, Emri M, et al. Application of computed tomography to assess the effect of egg yolk ratio on body composition in chickens of different genotype and gender at hatch and during the rearing period. *Br Poult Sci.* (2013) **54**:611–9. doi: 10.1080/00071668.2013.811714
44. Henning AL, Jiang MX, Yalcin HC, Butcher JT. Quantitative three-dimensional imaging of live avian embryonic morphogenesis via micro-computed tomography. *Dev Dyn.* (2011) **240**:1949–57. doi: 10.1002/dvdy.22694
45. Kim JS, Min J, Recknagel AK, Riccio M, Butcher JT. Quantitative three-dimensional analysis of embryonic chick morphogenesis via microcomputed tomography. *Anat Rec (Hoboken).* (2011) :1–10. doi: 10.1002/ar.21276
46. Metscher BD. MicroCT for developmental biology: a versatile tool for high-contrast 3D imaging at histological resolutions. *Dev Dyn.* (2009) **238**:632–40. doi: 10.1002/dvdy.21857
47. Chevalier NR, Dacher N, Jacques C, Langlois L, Guedj C, Faklaris O. Embryogenesis of the peristaltic reflex. *J Physiol.* (2019) **597**:2785–801. doi: 10.1113/JP277746
48. Lindner T, Klose R, Streckenbach F, Stahnke T, Hadlich S, Kuhn JP, et al. Morphologic and biometric evaluation of chick embryo eyes in ovo using 7 Tesla MRI. *Sci Rep.* (2017) **7**:2647. doi: 10.1038/s41598-017-02755-4
49. Zhou Z, Chen Z, Shan J, Ma W, Li L, Zu J, et al. Monitoring brain development of chick embryos in vivo using 3.0 T MRI: subdivision volume change and preliminary structural quantification using DTI. *BMC Dev Biol.* (2015) **15**:29. doi: 10.1186/s12861-015-0077-6
50. Boss A, Oppitz M, Wehrl HF, Rossi C, Feuerstein M, Claussen CD, et al. Measurement of T1, T2, and magnetization transfer properties during embryonic development at 7 Tesla using the chicken model. *J Magn Reson Imaging.* (2008) **28**:1510–4. doi: 10.1002/jmri.21601
51. Bain MM, Fagan AJ, Mullin JM, McNaught I, McLean J, Condon B. Noninvasive monitoring of chick development in ovo using a 7T MRI system from day 12 of incubation through to hatching. *J Magn Reson Imaging.* (2007) **26**:198–201. doi: 10.1002/jmri.20963
52. Hogers B, Gross D, Lehmann V, de Groot HJ, de Roos A, Gittenberger-de Groot AC, et al. Magnetic resonance microscopy at 17.6-Tesla on chicken embryos in vitro. *J Magn Reson Imaging.* (2001) **14**:83–6. doi: 10.1002/jmri.1155
53. Falen SW, Szeverenyi NM, Packard DS, Jr., Ruocco MJ. Magnetic resonance imaging study of the **structure** of the yolk in the developing avian egg. *J Morphol.* (1991) 209:331–42. doi: 10.1002/jmor.1052090308
54. Moseley ME, Wendland MF, Darnell DK, Gooding CA. Metabolic and anatomic development of the chick embryo as studied by phosphorus-31 magnetic resonance spectroscopy and proton MRI. *Pediatr Radiol.* (1989) **19**:400–5. doi: 10.1007/BF02387637
55. Streckenbach F, Klose R, Langner S, Langner I, Frank M, Wree A, et al. Ultrahigh-field quantitative mr microscopy of the chicken eye in vivo throughout the in ovo period. *Mol Imaging Biol.* (2019) **21**:78–85. doi: 10.1007/s11307-018-1208-9
56. Klose R, Streckenbach F, Hadlich S, Stahnke T, Guthoff R, Wree A, et al. [Ultra-high-field MRI in the Chicken Embryo in Ovo - a Model for Experimental Ophthalmology]. *Klin Monbl Augenheilkd.* (2017) **234**:1458–62. doi: 10.1055/s-0043-120675
57. Goodall N, Kisiswa L, Prashar A, Faulkner S, Tokarczuk P, Singh K, et al. 3-Dimensional modelling of chick embryo eye development and growth using high resolution magnetic resonance imaging. *Exp Eye Res.* (2009) **89**:511–21. doi: 10.1016/j.exer.2009.05.014
58. Herrmann A, Taylor A, Murray P, Poptani H, See V. Magnetic resonance imaging for characterization of a chick

embryo model of cancer cell metastases. *Mol Imaging.* (2018) **17**:1536012118809585. doi: 10.1177/1536012118809585
59. Shrivastava S, Barmon D, Kataki AC, Deka P, Sharma JD, Choudhary BK, et al. Magnetic resonance imaging in pre-operative staging of endometrial cancer. *Indian J Cancer.* (2016) **53**:181–5. doi: 10.4103/0019-509X.180859
60. Tung YT, Huang PW, Chou YC, Lai CW, Wang HP, Ho HC, et al. Lung tumorigenesis induced by human vascular endothelial growth factor (hVEGF)-A165 overexpression in transgenic mice and amelioration of tumor formation by miR-16. *Oncotarget.* (2015) **6**:10222–38. doi: 10.18632/oncotarget.3390
61. Zuo Z, Syrovets T, Genze F, Abaei A, Ma G, Simmet T, et al. High-resolution MRI analysis of breast cancer xenograft on the chick chorioallantoic membrane. *NMR Biomed.* (2015) **28**:440–7. doi: 10.1002/nbm.3270
62. Al-Mutawa YK, Herrmann A, Corbishley C, Losty PD, Phelan M, See V. Effects of hypoxic preconditioning on neuroblastoma tumour oxygenation and metabolic signature in a chick embryo model. *Biosci Rep.* (2018) **38**:185. doi: 10.1042/BSR20180185
63. Herrmann A, Rice M, Levy R, Pizer BL, Losty PD, Moss D, et al. Cellular memory of hypoxia elicits neuroblastoma metastasis and enables invasion by non-aggressive neighbouring cells. *Oncogenesis.* (2015) **4**:e138. doi: 10.1038/oncsis.2014.52
64. Kumar V, Nag TC, Sharma U, Mewar S, Jagannathan NR, Wadhwa S. High resolution 1H NMR-based metabonomic study of the auditory cortex analogue of developing chick (Gallus gallus domesticus) following prenatal chronic loud music and noise exposure. *Neurochem Int.* (2014) **76**:99–108. doi: 10.1016/j.neuint.2014.07.002
65. Zuo Z, Syrovets T, Wu Y, Hafner S, Vernikouskaya I, Liu W, et al. The CAM cancer xenograft as a model for initial evaluation of MR labelled compounds. *Sci Rep.* (2017) **7**:46690. doi: 10.1038/srep46690
66. Goodfellow F, Simchick GA, Mortensen LJ, Stice SL, Zhao Q. Tracking and quantification of magnetically labeled stem cells using magnetic resonance imaging. *Adv Funct Mater.* (2016) **26**:3899–915. doi: 10.1002/adfm.201504444
67. Pereira SM, Herrmann A, Moss D, Poptani H, Williams SR, Murray P, et al. Evaluating the effectiveness of transferrin receptor-1 (TfR1) as a magnetic resonance reporter gene. *Contrast Media Mol Imaging.* (2016) **11**:236–44. doi: 10.1002/cmmi.1686
68. Zlatopolskiy BD, Zischler J, Schafer D, Urusova EA, Guliyev M, Bannykh O, et al. Discovery of 7-[(18)F]Fluorotryptophan as a novel positron emission tomography (PET) probe for the visualization of tryptophan metabolism *in vivo*. *J Med Chem.* (2018) **61**:189–206. doi: 10.1021/acs.jmedchem.7b01245
69. Warnock G, Turtoi A, Blomme A, Bretin F, Bahri MA, Lemaire C, et al. In vivo PET/CT in a human glioblastoma chicken chorioallantoic membrane model: a new tool for oncology and radiotracer development. *J Nucl Med.* (2013) **54**:1782–8. doi: 10.2967/jnumed.112.117150
70. Gebhardt P, Wurbach L, Heidrich A, Heinrich L, Walther M, Opfermann T, et al. Dynamic behaviour of selected PET tracers in embryonated chicken eggs. *Rev Esp Med Nucl Imagen Mol.* (2013) **32**:371–7. doi: 10.1016/j.remnie.2013.09.013
71. Wurbach L, Heidrich A, Opfermann T, Gebhardt P, Saluz HP. Insights into bone metabolism of avian embryos in ovo via 3D and 4D 18F-fluoride positron emission tomography. *Mol Imaging Biol.* (2012) **14**:688–98. doi: 10.1007/s11307-012-0550-6
72. Fiebig HH, Maier A, Burger AM. Clonogenic assay with established human tumour xenografts: correlation of in vitro to in vivo activity as a basis for anticancer drug discovery. *Eur J Cancer.* (2004) **40**:802–20. doi: 10.1016/j.ejca.2004.01.009
73. Landis MD, Lehmann BD, Pietenpol JA, Chang JC. Patient-derived breast tumor xenografts facilitating personalized cancer therapy. *Breast Cancer Res.* (2013) **15**:201. doi: 10.1186/bcr3355
74. de Bono JS, Ashworth A. Translating cancer research into targeted therapeutics. *Nature.* (2010) **467**:543–9. doi: 10.1038/nature09339
75. Tentler JJ, Tan AC, Weekes CD, Jimeno A, Leong S, Pitts TM, et al. Patient-derived tumour xenografts as models for oncology drug development. *Nat Rev Clin Oncol.* (2012) **9**:338–50. doi: 10.1038/nrclinonc.2012.61
76. Rosfjord E, Lucas J, Li G, Gerber HP. Advances in patient-derived tumor xenografts: from target identification to predicting clinical response rates in oncology. *Biochem Pharmacol.* (2014) **91**:135–43. doi: 10.1016/j.bcp.2014.06.008
77. Galuschka C, Proynova R, Roth B, Augustin HG, Muller-Decker K. Models in translational oncology: a public resource database for preclinical cancer research. *Cancer Res.* (2017) **77**:2557–63. doi: 10.1158/0008-5472.CAN-16-3099
78. Lokman NA, Elder AS, Ricciardelli C, Oehler MK. Chick chorioallantoic membrane (CAM) assay as an in vivo model to study the effect of newly identified molecules on ovarian cancer invasion and metastasis. *Int J Mol Sci.* (2012) **13**:9959–70. doi: 10.3390/ijms13089959
79. Ribatti D. The chick embryo chorioallantoic membrane (CAM) assay. *Reprod Toxicol.* (2017) **70**:97–101. doi: 10.1016/j.reprotox.2016.11.004
80. Hamburger V, Hamilton HL. A series of normal stages in the development of the chick embryo. *J Morphol.* (1951) **88**:49–92. doi: 10.1002/jmor.1050880104
81. Bone SN, Johnson GA, Thompson MB. Three-dimensional magnetic resonance microscopy of the developing chick embryo. *Invest Radiol.* (1986) **21**:782–7. doi: 10.1097/00004424-198610000-00003
82. Johnson GA, Thompson MB, Drayer BP, Bone SN. Magnetic resonance microscopy in neurologic models. *Acta Radiol Suppl.* (1986) **369**:267–8.
83. Effmann EL, Johnson GA, Smith BR, Talbott GA, Cofer G. Magnetic resonance microscopy of chick embryos in ovo. *Teratology.* (1988) **38**:59–65. doi: 10.1002/tera.1420380109
84. Hollett MD, Cofer GP, Johnson GA. In situ magnetic resonance microscopy. *Invest Radiol.* (1987) **22**:965–8. doi: 10.1097/00004424-198712000-00009
85. Lirette A, Towner RA, Liu Z EG, Janzen. Chambers JR, Fairfull RW, Milligan LP, et al. In vivo nuclear magnetic resonance spectroscopy of chicken embryos from two broiler strains of varying fat content. *Poult Sci.* (1993) **72**:1411–20. doi: 10.3382/ps.0721411
86. Peebles DM, Dixon JC, Thornton JS, Cady EB, Priest A, Miller SL, et al. Magnetic resonance proton spectroscopy and diffusion weighted imaging of chick embryo brain in ovo. *Brain Res Dev Brain Res.* (2003) **141**:101–7. doi: 10.1016/S0165-3806(03)00002-6
87. Hutchison MJ, Lirette A, Etches RJ, Towner RA, Janzen EG. Research note: an assessment of egg yolk structure using magnetic resonance imaging. *Poult Sci.* (1992) **71**:2117–21. doi: 10.3382/ps.0712117
88. Donoghue DJ, Myers K. Imaging residue transfer into egg yolks. *J Agric Food Chem.* (2000) **48**:6428–30. doi: 10.1021/jf000146h
89. Smith BR, Effmann EL, Johnson GA. MR microscopy of chick embryo vasculature. *J Magn Reson Imaging.* (1992) **2**:237–40. doi: 10.1002/jmri.1880020220
90. Zhang X, Yelbuz TM, Cofer GP, Choma MA, Kirby ML, Johnson GA. Improved preparation of chick embryonic samples for magnetic resonance microscopy. *Magn Reson Med.* (2003) **49**:1192–5. doi: 10.1002/mrm.10460
91. Yelbuz TM, Zhang X, Choma MA, Stadt HA, Zdanowicz M, Johnson GA, et al. Images in cardiovascular medicine. Approaching cardiac development in three dimensions by magnetic resonance microscopy. *Circulation.* (2003) **108**:e154–5. doi: 10.1161/01.CIR.0000102940.17908.CA
92. Yelbuz TM, Waldo KL, Zhang X, Zdanowicz M, Parker J, Creazzo TL, et al. Myocardial volume and organization are changed by failure of addition of secondary heart field myocardium to the cardiac outflow tract. *Dev Dyn.* (2003) **228**:152–60. doi: 10.1002/dvdy.10364
93. Holmes WM, McCabe C, Mullin JM, Condon B, Bain MM. Images in cardiovascular medicine. Noninvasive self-gated magnetic resonance cardiac imaging of developing chick embryos in ovo. *Circulation.* (2008) **117**:e346–7. doi: 10.1161/CIRCULATIONAHA.107.747154
94. Holmes WM, McCabe C, Mullin JM, Condon B, Bain MM. In ovo non-invasive quantification of the myocardial function and mass of chick embryos using magnetic resonance imaging. *NMR Biomed.* (2009) **22**:745–52. doi: 10.1002/nbm.1386
95. Li X, Liu J, Davey M, Duce S, Jaberi N, Liu G, et al. Micro-magnetic resonance imaging of avian embryos. *J Anat.* (2007) **211**:798–809. doi: 10.1111/j.1469-7580.2007.00825.x
96. Goodfellow FT, Tesla B, Simchick G, Zhao Q, Hodge T, Brindley MA, et al. Zika virus induced mortality and microcephaly in chicken embryos. *Stem Cells Dev.* (2016) **25**:1691–7. doi: 10.1089/scd.2016.0231

97. Dingman S, Hurlburt L, Thomas R, Guo C. Tissue immunoassay for 19F-tagged 5-hydroxytryptophan. *J Immunoassay Immunochem.* (2003) 24:325–44. doi: 10.1081/IAS-120025771
98. Oppitz M, Pintaske J, Kehlbach R, Schick F, Schriek G, Busch C. Magnetic resonance imaging of iron-oxide labeled SK-Mel 28 human melanoma cells in the chick embryo using a clinical whole body MRI scanner. *MAGMA.* (2007) **20**:1–9. doi: 10.1007/s10334-006-0062-y
99. Pereira SM, Moss D, Williams SR, Murray P, Taylor A. Overexpression of the MRI reporter genes ferritin and transferrin receptor affect iron homeostasis and produce limited contrast in mesenchymal stem cells. *Int J Mol Sci.* (2015) **16**:15481–96. doi: 10.3390/ijms160715481
100. Faucher L, Guay-Begin AA, Lagueux J, Cote MF, Petitclerc E, Fortin MA. Ultra-small gadolinium oxide nanoparticles to image brain cancer cells in vivo with MRI. *Contrast Media Mol Imaging.* (2011) **6**:209–18. doi: 10.1002/cmmi.420
101. Taylor A, Herrmann A, Moss D, See V, Davies K, Williams SR, et al. Assessing the efficacy of nano- and micro-sized magnetic particles as contrast agents for MRI cell tracking. *PLoS ONE.* (2014) **9**:e100259. doi: 10.1371/journal.pone.0100259
102. Hafner S, Raabe M, Wu Y, Wang T, Zuo Z, Rasche V, et al. High-contrast magnetic resonance imaging and efficientdelivery of an albumin nanotheranostic in triple-negativebreast cancer xenografts. *Adv Therap.* (2019) **2**:1900084. doi: 10.1002/adtp.201900084
103. Buschmann J, Welti M, Hemmi S, Neuenschwander P, Baltes C, Giovanoli P, et al. Three-dimensional co-cultures of osteoblasts and endothelial cells in DegraPol foam: histological and high-field magnetic resonance imaging analyses of pre-engineered capillary networks in bone grafts. *Tissue Eng Part A.* (2011) **17**:291–9. doi: 10.1089/ten.tea.2010.0278
104. Chesnick IE, Fowler CB, Mason JT, Potter K. Novel mineral contrast agent for magnetic resonance studies of bone implants grown on a chick chorioallantoic membrane. *Magn Reson Imaging.* (2011) **29**:1244–54. doi: 10.1016/j.mri.2011.07.022
105. Kivrak Pfiffner F, Waschkies C, Tian Y, Woloszyk A, Calcagni M, Giovanoli P, et al. A new in vivo magnetic resonance imaging method to noninvasively monitor and quantify the perfusion capacity of three-dimensional biomaterials grown on the chorioallantoic membrane of chick embryos. *Tissue Eng Part C Methods.* (2015) **21**:339–46. doi: 10.1089/ten.tec.2014.0212
106. Waschkies C, Nicholls F, Buschmann J. Comparison of medetomidine, thiopental and ketamine/midazolam anesthesia in chick embryos for in ovo Magnetic Resonance Imaging free of motion artifacts. *Sci Rep.* (2015) **5**:15536. doi: 10.1038/srep15536
107. Heidrich A, Wurbach L, Opfermann T, Saluz HP. Motion-artifact-free in vivo imaging utilizing narcotized avian embryos in ovo. *Mol Imaging Biol.* (2011) **13**:208–14. doi: 10.1007/s11307-010-0355-4
108. Freesmeyer M, Kuehnel C, Opfermann T, Niksch T, Wiegand S, Stolz R, et al. The use of ostrich eggs for in ovo research: making preclinical imaging research affordable and available. *J Nucl Med.* (2018) **59**:1901–6. doi: 10.2967/jnumed.118.210310
109. Steinemann G, Dittmer A, Schmidt J, Josuttis D, Fahling M, Biersack B, et al. Antitumor and antiangiogenic activity of the novel chimeric inhibitor animacroxam in testicular germ cell cancer. *Mol Oncol.* (2019) **13**:2679–96. doi: 10.1002/1878-0261.12582
110. Winter G, Koch A, Subgang A, Solbach C, Glatting G, Rasche V, et al. Evaluation of binding specificity of target-specific radioligands in xenografts by multi-modal PET and MR imaging using the Hen's egg test chorioallantoic membrane (HET-CAM) model. *J Nucl Med.* (2019) **16**:1003.
111. Zhou Z, Xu J, Delproposto ZS, Hua J, Fan Y, Zhang Z, et al. Feasibility of in ovo diffusion tractography in the chick embryo using a dual-cooling technique. *J Magn Reson Imaging.* (2012) **36**:993–1001. doi: 10.1002/jmri.23684
112. Dingman S, Hurlburt L, Branch C. Acute no-effect dose for in ova exposure to C3F7 tagged 5-hydroxytryptophan, a novel probe for investigating neural development. *Mol Imaging Biol.* (2004) **6**:12–6. doi: 10.1016/j.mibio.2003.11.001
113. Tazawa H, Rahn H. Temperature and metabolism of chick embryos and hatchlings after prolonged cooling. *J Exp Zool Suppl.* (1987) **1**:105–9.
114. Wojtczak JA. The hemodynamic effects of halothane and isoflurane in chick embryo. *Anesth Analg.* (2000) **90**:1331–5. doi: 10.1097/00000539-200006000-00012
115. Berry DG. Effect of ketamine on the isolated chick embryo heart. *Anesth Analg.* (1974) **53**:919–23. doi: 10.1213/00000539-197453060-00021
116. Kulesa PM, Bailey CM, Cooper C, Fraser SE. In ovo live imaging of avian embryos. *Cold Spring Harb Protoc.* (2010) **2010**:pdb prot5446. doi: 10.1101/pdb.prot5446
117. Canaria CA, Lansford R. Advanced optical imaging in living embryos. *Cell Mol Life Sci.* (2010) **67**:3489–97. doi: 10.1007/s00018-010-0440-5
118. Jefferies B, Tong Z, Nawroth R. Bioluminescence imaging in the chick chorioallantoic membrane assay. *Methods Mol Biol.* (2020) **2081**:211–7. doi: 10.1007/978-1-4939-9940-8_15
119. Jefferies B, Lenze F, Sathe A, Truong N, Anton M, von Eisenhart-Rothe R, et al. Non-invasive imaging of engineered human tumors in the living chicken embryo. *Sci Rep.* (2017) **7**:4991. doi: 10.1038/s41598-017-04572-1
120. Raghunathan R, Singh M, Dickinson ME, Larin KV. Optical coherence tomography for embryonic imaging: a review. *J Biomed Opt.* (2016) **21**:50902. doi: 10.1117/1.JBO.21.5.050902
121. Teddy JM, Lansford R, Kulesa P. Four-color M, 4-D time-lapse confocal imaging of chick embryos. *Biotechniques.* (2005) **39**:703–10. doi: 10.2144/000112017
122. McQuinn TC, Bratoeva M, Dealmeida A, Remond M, Thompson RP, Sedmera D. High-frequency ultrasonographic imaging of avian cardiovascular development. *Dev Dyn.* (2007) **236**:3503–13. doi: 10.1002/dvdy.21357
123. Sharma A, Ishak N, Swee-Hin T, Pramanik M. High resolution, label-free photoacoustic imaging of live chicken embryo developing in bioengineered eggshell. *J Biophotonics.* (2020) **13**:e201960108. doi: 10.1002/jbio.201960108

Conflict of Interest: The authors declare that the research was conducted in the absence of any commercial or financial relationships that could be construed as a potential conflict of interest.